SDAC-TR-76-9

(12)

STUDY OF SELECTED EVENTS IN THE TIEN SHAN REGION IN A SEISMIC DISCRIMINATION CONTEXT

P.A. Sobel and D.H. von Seggern
Seismic Data Analysis Center
Teledyne Geotech, 314 Montgomery Street, Alexandria, Virginia 22314

26 AUGUST 1976

Sponsored By
The Defense Advanced Research Projects Agency
Nuclear Monitoring Research Office
1400 Wilson Boulevard, Arlington, Virginia 22209
ARPA Order No. 1620

Monitored By
VELA Seismological Center
312 Montgomery Street, Alexandria, Virginia 22314

21 Apr 77 1st
Mrs Spring, ARPA
tele 694 5920

1- ARPA Order - 1620
2- ARPA Order - 2551
Q. which is the correct order
no for this report

A. No. 2 is correct.
mt.

Unclassified

SECURITY CLASSIFICATION OF THIS PAGE (When Data Entered)

REPORT DOCUMENTATION PAGE

READ INSTRUCTIONS BEFORE COMPLETING FORM

1. REPORT NUMBER: SDAC-TR-76-9
2. GOVT ACCESSION NO.:
3. RECIPIENT'S CATALOG NUMBER:

4. TITLE (and Subtitle): STUDY OF SELECTED EVENTS IN THE TIEN SHAN REGION IN A SEISMIC DISCRIMINATION CONTEXT.

5. TYPE OF REPORT & PERIOD COVERED: Technical rept.

6. PERFORMING ORG. REPORT NUMBER:

7. AUTHOR(s): P. A. Sobel, D. H. von Seggern

8. CONTRACT OR GRANT NUMBER(s): F08606-76-C-0004, ARPA Order-2551

9. PERFORMING ORGANIZATION NAME AND ADDRESS: Teledyne Geotech, 314 Montgomery Street, Alexandria, Virginia 22314

10. PROGRAM ELEMENT, PROJECT, TASK AREA & WORK UNIT NUMBERS: VT/6709

11. CONTROLLING OFFICE NAME AND ADDRESS: Defense Advanced Research Projects Agency, Nuclear Monitoring Research Office, 1400 Wilson Blvd. Arlington, Virginia 22209

12. REPORT DATE: 08/26/76

13. NUMBER OF PAGES: 78

14. MONITORING AGENCY NAME & ADDRESS (if different from Controlling Office): VELA Seismological Center, 312 Montgomery Street, Alexandria, Virginia 22314

15. SECURITY CLASS. (of this report): Unclassified

15a. DECLASSIFICATION/DOWNGRADING SCHEDULE:

16. DISTRIBUTION STATEMENT (of this Report)

17. DISTRIBUTION STATEMENT (of the abstract entered in Block 20, if different from Report)

APPROVED FOR PUBLIC RELEASE; DISTRIBUTION UNLIMITED.

18. SUPPLEMENTARY NOTES

19. KEY WORDS (Continue on reverse side if necessary and identify by block number)

Tien Shan
Lop Nor Test Site
Seismic Discrimination
Underground Nuclear Explosions
M_S versus m_b

20. ABSTRACT (Continue on reverse side if necessary and identify by block number)

Eleven earthquakes with low reported M_S for their m_b from the area near Lop Nor in the eastern Tien Shan were examined in a seismic discrimination context. Seismograms from ALPA, LASA, NORSAR, the HGLP and the WWSSN stations were studied for source mechanisms, M_S-m_b, corner frequency, long-period body-wave excitation, pP, complexity, spectral ratio, and S/P excitation. All the events can be identified as earthquakes except the October 27, 1975 event which exhibits explosion characteristics.

DD FORM 1 JAN 73 1473 EDITION OF 1 NOV 65 IS OBSOLETE

Unclassified 408 258

SECURITY CLASSIFICATION OF THIS PAGE (When Data Entered)

STUDY OF SELECTED EVENTS IN THE TIEN SHAN REGION IN A SEISMIC DISCRIMINATION CONTEXT

SEISMIC DATA ANALYSIS CENTER REPORT NO.: SDAC-TR-76-9

AFTAC Project Authorization No.:	VELA T/6709/B/ETR
Project Title:	Seismic Data Analysis Center
ARPA Order No.:	2551
ARPA Program Code No.:	6F10
Name of Contractor:	TELEDYNE GEOTECH
Contract No.:	F08606-76-C-0004
Date of Contract:	01 July 1975
Amount of Contract:	$2,319,926
Contract Expiration Date:	30 June 1976
Project Manager:	Royal A. Hartenberger (703) 836-3882

P. O. Box 334, Alexandria, Virginia 22314

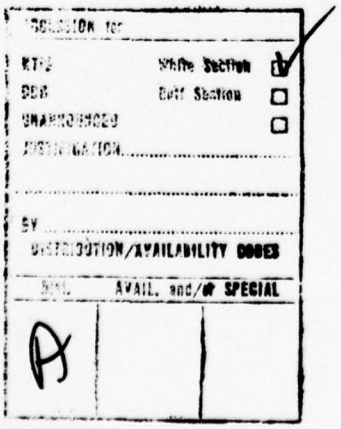

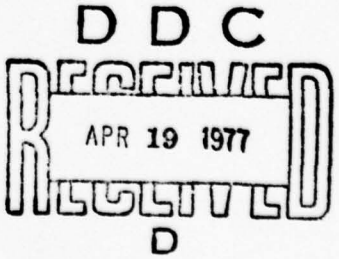

ABSTRACT

Eleven earthquakes with low reported M_s for their m_b from the area near Lop Nor in the eastern Tien Shan were examined in a seismic discrimination context. Seismograms from ALPA, LASA, NORSAR, the HGLP and the WWSSN stations were studied for source mechanisms, M_s-m_b, corner frequency, long-period body-wave excitation, pP, complexity, spectral ratio, and S/P excitation. All the events can be identified as earthquakes except the October 27, 1975 event which exhibits explosion characteristics.

TABLE OF CONTENTS

LIST OF FIGURES

LIST OF TABLES

INTRODUCTION

Discrimination parameters have been applied in detail at only a few nuclear test sites. In order to firmly establish the worth of various discriminants, it is necessary to extend these studies to other regions of shallow earthquakes. This report examines eleven earthquakes in the Tien Shan Region of China which had low reported M_s for their m_b, such that these events fall close to the explosion population on a M_s-m_b graph. The area of interest is shown in the inset of Figure 1. The Lop Nor area in the southeastern corner of the region of interest has been the testing site of several atmospheric and at least one known underground nuclear explosion. Most of the earthquakes in the Tien Shan area are probably associated with crustal faulting in the mountains which are currently undergoing uplift. Unfortunately the events chosen were too small to determine their fault plane mechanisms. Average M_s and m_b are independently determined for the events in this study. Common discrimination parameters such as first motions, corner frequency, and spectral ratios are applied to the data, and the Tien Shan events are compared to Kazakh explosions.

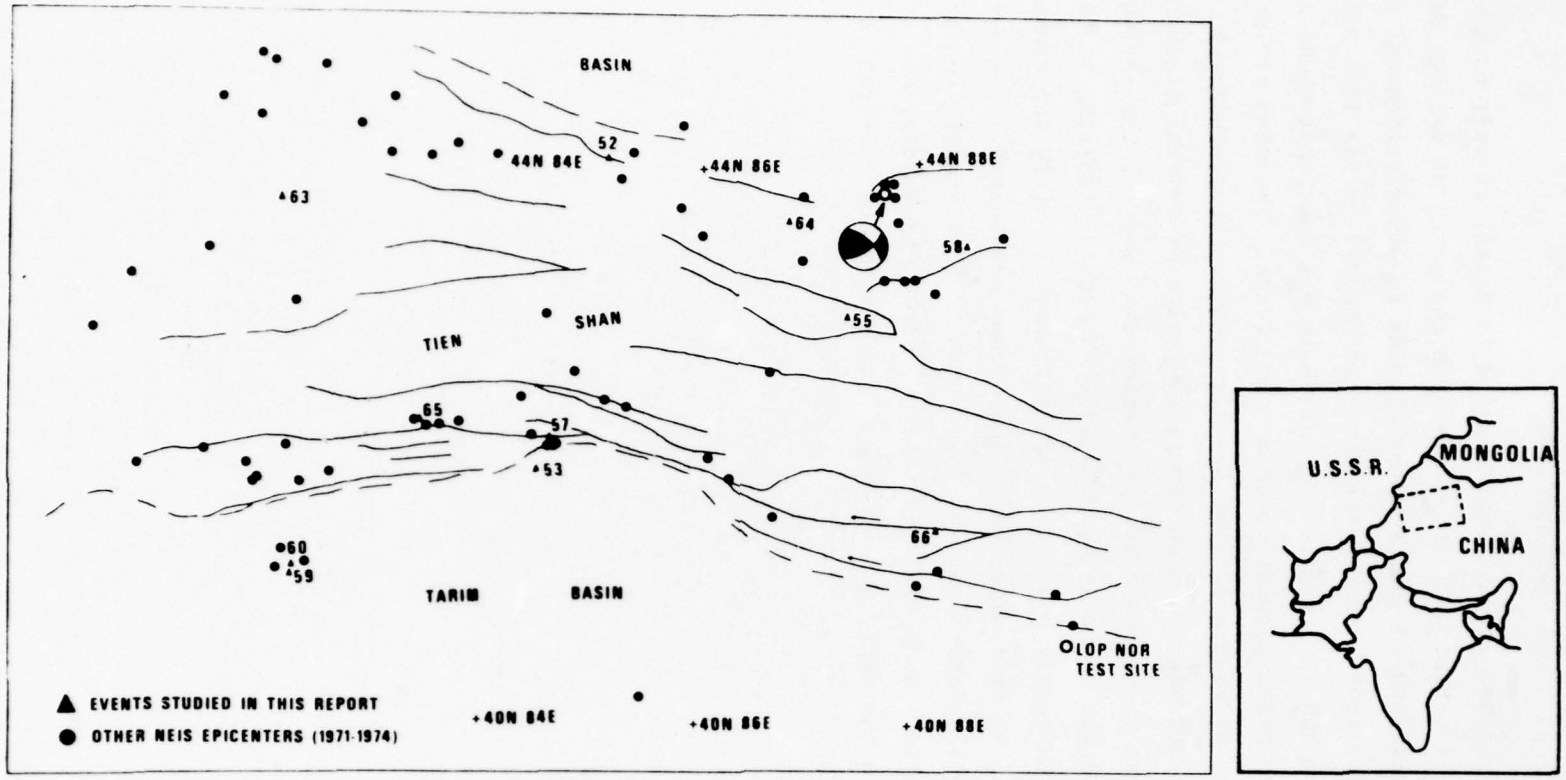

Figure 1. Map of Northern Sinkiang Province showing faults, 1961 to 1975 NEIS events and the focal mechanism of the November 13, 1965 earthquake. Inset shows area of interest. Faults are denoted by solid lines, tectonic boundaries by dashed lines, and events studied in this report by event numbers.

TECTONIC SETTING

General Features

Figure 1 shows the region of interest. Due to its remote location, little is known about the geology of Northern Sinkiang Province. Most of the known geologic information has been inferred from satellite photographs. The Tarim Basin, a Precambrian structure filled with glacial sediments, lies in the southern part of the region. The Tien Shan mountains, a part of the Eurasian arc system, lie in the northern part of the region. These mountains may have been a Paleozoic plate boundary and are now undergoing uplift as a result of the collision of the Indian and Asian plates (York, 1976; Molnar and Tapponnier, 1975).

Source Mechanisms of Earthquakes

Most of the earthquakes in this area are associated with the large subparallel left-lateral strike-slip faults which transect the mountains (York, 1976) or are an expression of the current uplift along thrust faults in the eastern Tien Shan (Zaychikov, 1965). Virtually no epicenters occur within the Tarim Basin. NEIS epicenters for events in this area from 1961 through 1975 are shown overlaying presumed faults in Figure 1. These presumed faults were inferred from our satellite photomosaic of the entire area. It can be seen that major faults are associated with most epicenters in this area. Two of the earthquakes studied here, events 59 and 60, occurred in the Tarim Basin and are not associated with any known faults. The Lop Nor test site for atmospheric explosions lies in the eastern part of the basin at approximately 41N, 90E. The only event found to have explosion characteristics, event 66, is also the closest of our events to the test site.

Studies of earthquake focal mechanisms in the Tien Shan have shown that the compressive stress axes were almost always horizontally oriented, perpendicular to the trend of the mountains and visible faults (Shirokova, 1967). Movements occur mainly along planes with steep dip angles. Both strike-slip and thrust movements are present. The fault plane mechanism for an earthquake near 44N, 88E is shown in Figure 1. The event occurred on November 13, 1965, at 04: 33: 53.0 (Molnar, 1973). It is not part of this study; however, its basically left-lateral strike-slip motion is probably typical of many earthquakes in this region.

Velocity Model

Seismic studies in the Tien Shan report an average crustal thickness of 50 to 60 Km (Volarovich, 1975; Belyaevsky, 1973). The average crustal thickness in the Tarim Basin is 40 to 50 km (Belyaevsky, 1973). Table I shows the crustal and upper mantle velocity structure derived from deep seismic sounding in the Tien Shan (Volarovich, 1975). The agreement between ISC computed and LASA and NORSAR pP depths in Table II implies that the Jeffreys-Bullen Travel-time tables are well suited to locating events in this region. Moreover, since these tables require an earth model with significantly shallower crust and higher P-wave velocities between 30 and 50 km than the Tien Shan model, it can be concluded that the actual upper mantle below this region has velocities at least as great as those in J-B model, or in other words, that there is no appreciable low-velocity zone. This conclusion implies that P-wave attenuation should be relatively weak.

TABLE I

VELOCITY STRUCTURE IN THE TIEN SHAN MOUNTAINS

THICKNESS (KM)	P VELOCITY (KM/SEC)
10	6.0
10	6.3
10	6.4
10	6.4
10	6.5
10	8.0

DATA

Earthquakes Selection

For this report earthquakes were selected which had low reported M_s for their m_b so that these events fell close to the explosion population on an M_s-m_b graph. The Northern Sinkiang Province contains mostly shallow (less than 70 km) depth events; this conclusion is suggested by depths found in the NEIS list. The earthquakes chosen were limited to the years 1971-1975 so that we could utilize data from the large seismic arrays and the HGLP network data. We selected a total of 11 earthquakes as listed in Table II and shown in Figure 1. Table II also lists the ISC depths for 7 of the events; no ISC data were available for the other 4 events at the time of this study. These ISC depths agree to within 5 km of the depths determined from pP observations at LASA and NORSAR except for the event on 17 May 1973 with a focal depth of 96 km. Apparently this depth was assigned, not computed, by the ISC for an unknown reason; and it is evident from the pattern of travel-time residuals in the ISC bulletin that a shallower depth for this event would probably reduce the variance of the residuals. Our analysis of signals from this event revealed clear pP phases at four stations, giving an average depth of 23 km with small scatter. Thus we feel that this epicenter is shallow, in accord with the general seismicity pattern of this region where few events have been reported with depths below 70 km (which reported depths may be erroneous anyway). Reinforcing this conclusion is the proximity of event 60 to event 59, which has a reported focal depth of 3 km.

Seismic Stations

Digital data from the three large arrays ALPA, LASA, and NORSAR and from the available HGLP stations and film data from WWSSN stations were gathered for these events. A high percentage of the HGLP data could not be recovered or were not usuable, and many WWSSN film chips were not available for the 1975 events.

TABLE II

NEIS PARAMETERS FOR TIEN SHAN EARTHQUAKES

EVENT	DATE	ORIGIN TIME	LATITUDE N	LONGITUDE E	m_b	DEPTH NEIS	DEPTH ISC	DEPTH LASA	DEPTH NORSAR
52	01 NOV 71	05 29 57.2	44.042	85.050	5.0	33	30		33
53	02 JAN 72	10 27 34.9	41.800	84.472	5.2	33	11	11	11
55	24 MAR 72	08 11 52.8	42.943	87.438	5.0	33	39	23	24
57	20 APR 72	00 35 56.7	42.005	84.583	5.1	33	20	25	22
58	10 JUL 72	19 03 33.0	43.440	88.629	4.7	33	36		41
59	24 JAN 73	03 20 20.2	40.957	82.183	5.1	33	3	5	17
60	17 MAY 73	09 38 09.9	41.025	82.195	5.5	33	96		
63	03 NOV 74	10 27 31.0	43.627	81.866	5.2	33		32	
64	14 JAN 75	14 13 49.8	43.622	86.870	5.0	33			42
65	22 FEB 75	05 03 38.2	42.112	83.329	5.0	33		16	17
66	27 OCT 75	01 00 03.5	41.397	88.291	5.0	33		0	0

SIGNAL ANALYSIS

Source Effects

We wanted initially to identify a source mechanism for each event so that we could predict the radiation pattern for body-wave and surface-wave phases. Determination of the fault planes for earthquakes whose magnitude are below 6.0 is generally not reliable with teleseismic data, and all our earthquakes have m_b less than 6. The epicenters occur near faults that are inferred to be thrust and strike-slip faults from the satellite photographs or other sources; and thus we cannot assume a common mechanism for all the events. We have plotted first motions taken from ISC short-period data in Figure 2. No data were available for the four most recent events. Only a few long-period first motions could be determined from the WWSSN for these events and they were not added to Figure 2. Unfortunately the short-period data were not good, and it is impossible on the basis of these plots alone to determine fault planes because dilatational and compressional first motions do not separate.

Corner frequencies and moments for our Tien Shan events have been estimated from short-period LASA and NORSAR spectra. The spectra of several of the events are shown in Figure 3. These spectra are from the phased beams of the A0 short-period subarray at LASA and C3 short-period subarray at NORSAR. The sample length was 25.6 seconds. The signals have been tapered, and the instrument response removed from the signal spectra but not the noise spectra; noise spectra have not been subtracted from the signal spectra. Attenuation was removed from the signal spectra by multiplying by the factor $\exp[\pi f t^*]$ with a t^* of .44 for LASA and .20 for NORSAR. The basis of these t^* values will be shown later in this report. Corner frequencies were estimated with the assumption of complete stress drop and a ω^{-2} or ω^{-3} asymptotic relation at high frequencies. All the spectra at LASA drop off at roughly ω^{-3} above the corner frequency but most of the NORSAR spectra drop off at ω^{-2}, implying that the t^* values we calculated are incorrect for at least one of the two paths.

Seismic moment was calculated from the long-period spectral levels $|\hat{u}_o|$ estimated in Figure 3 using the relation (Hanks and Thatcher, 1972)

$$M_o = 4\pi\rho\alpha^3 |\hat{u}_o| R_{\theta\phi} D$$

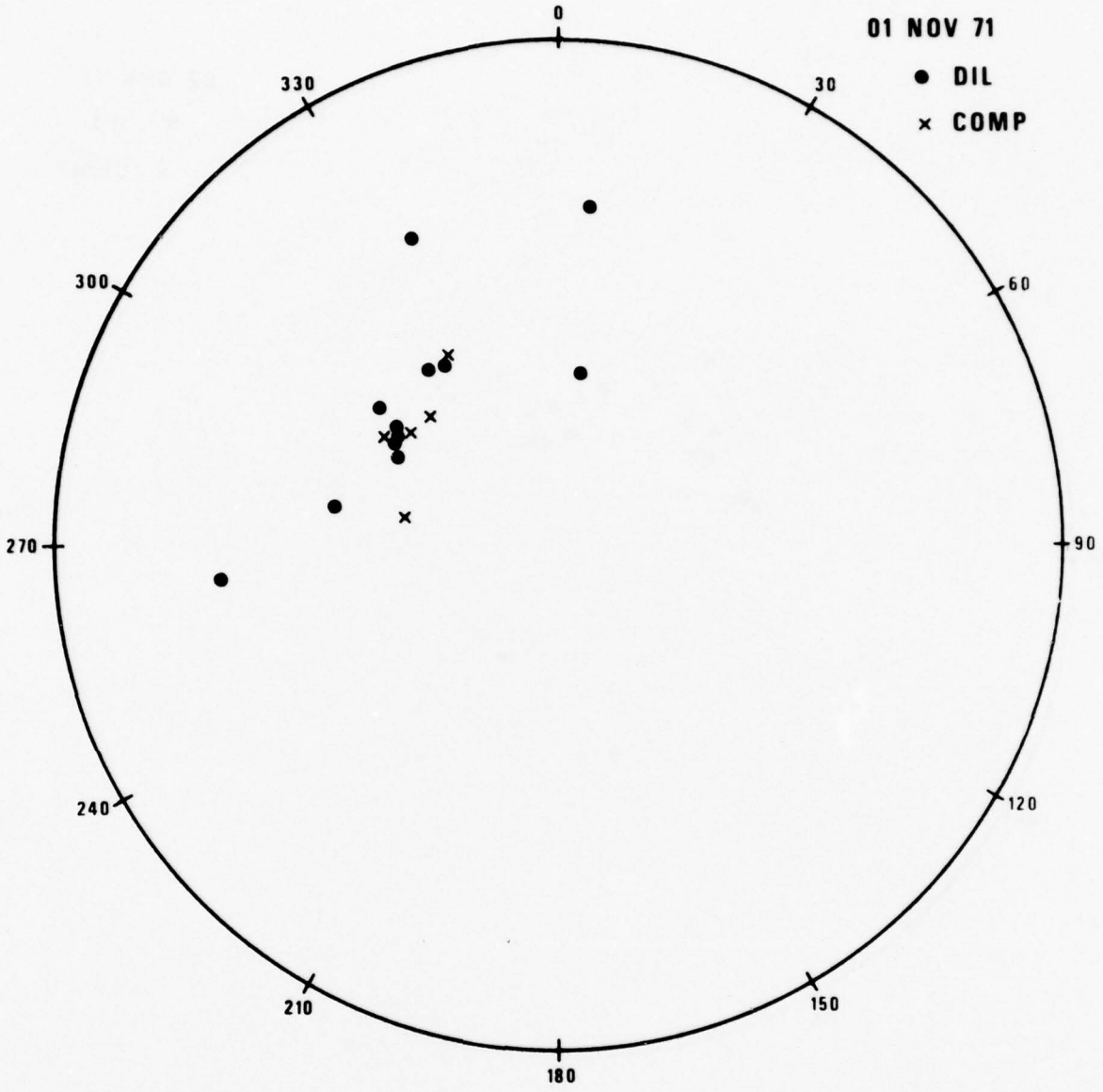

Figure 2. First motions for Tien Shan earthquakes in the lower half of the focal sphere (Wulff net).

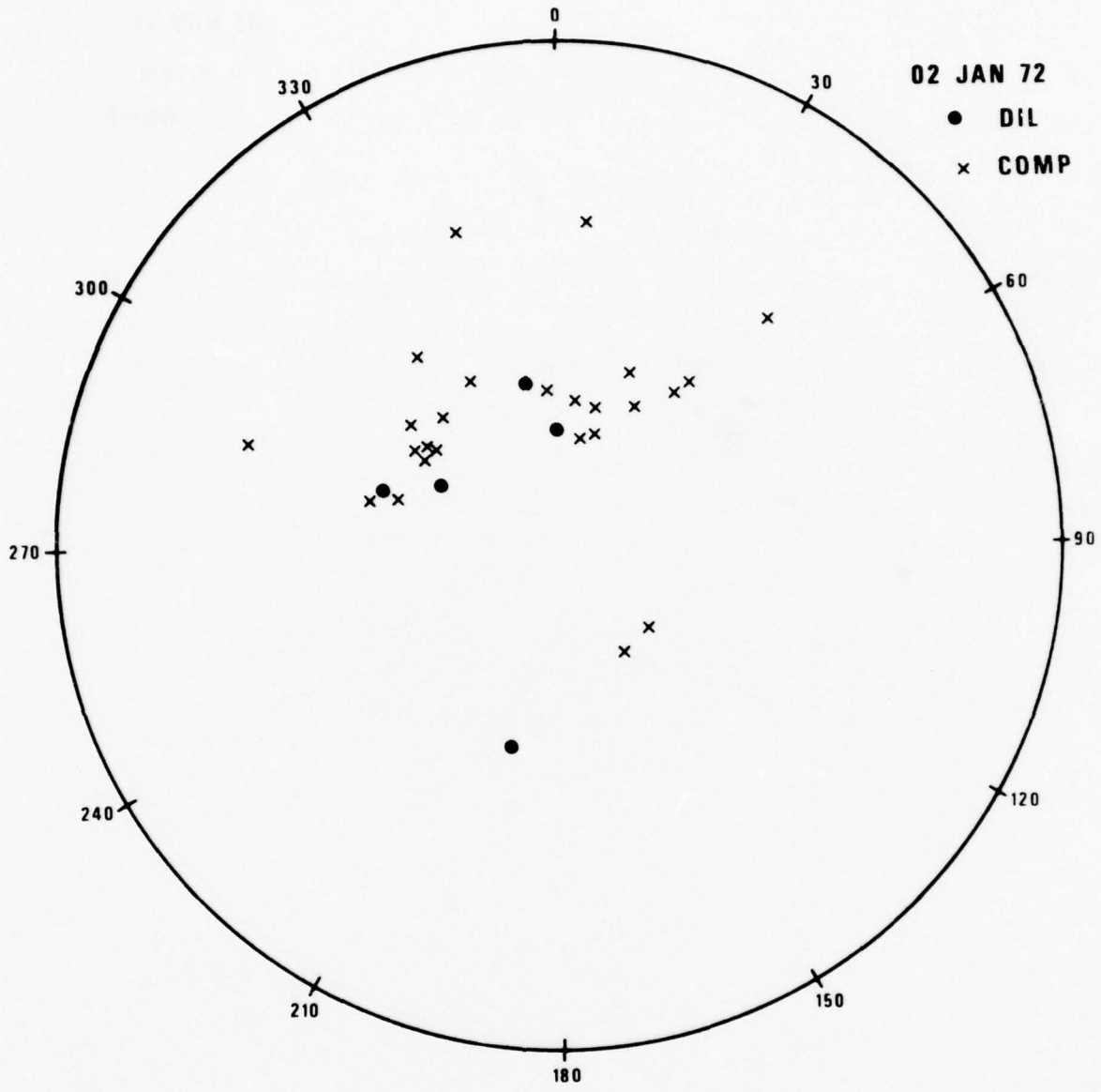

Figure 2 (Continued). First motions for Tien Shan earthquakes in the lower half of the focal sphere (Wulff net).

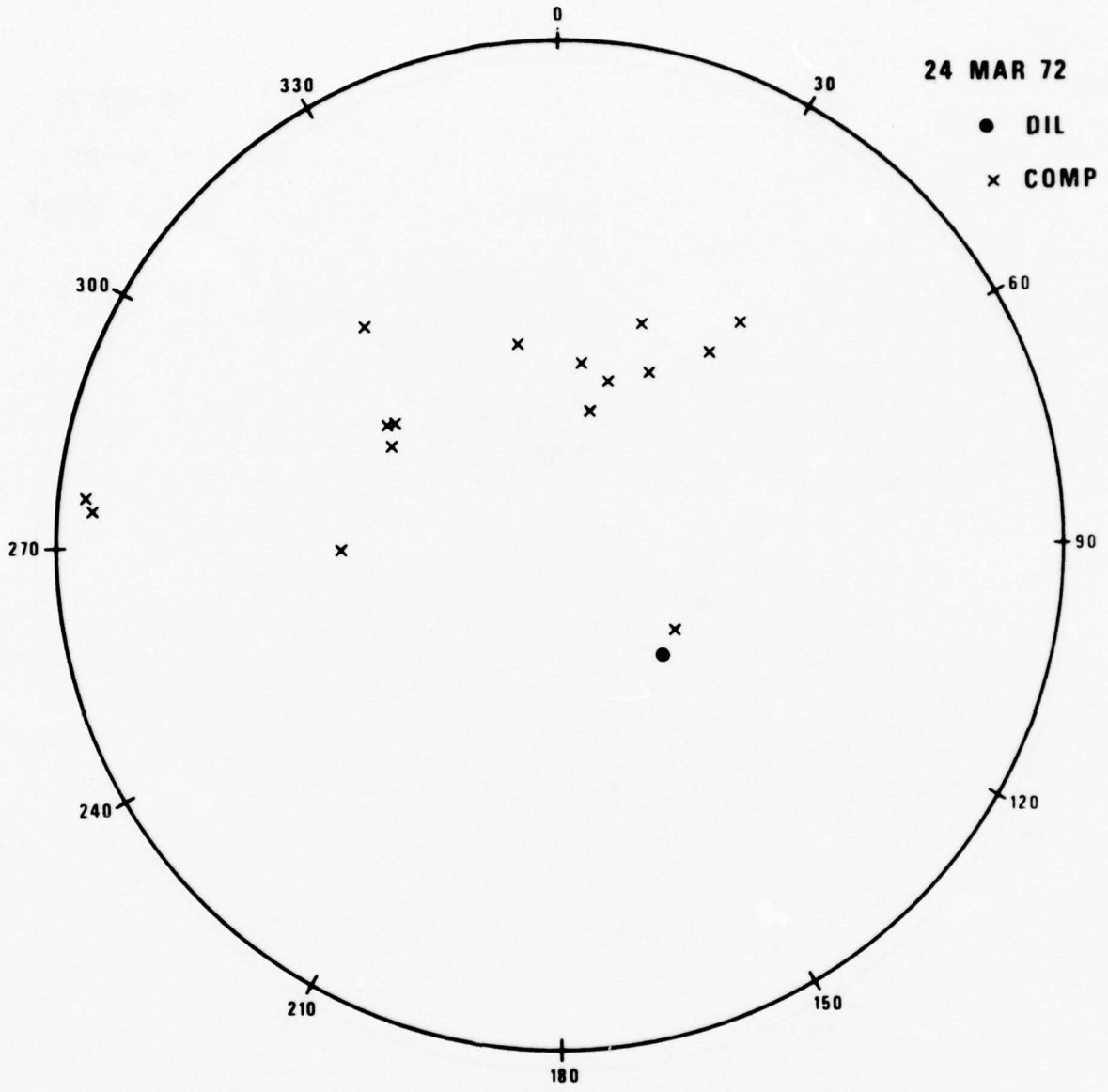

Figure 2 (Continued). First motions for Tien Shan earthquakes in the lower half of the focal sphere (Wulff net).

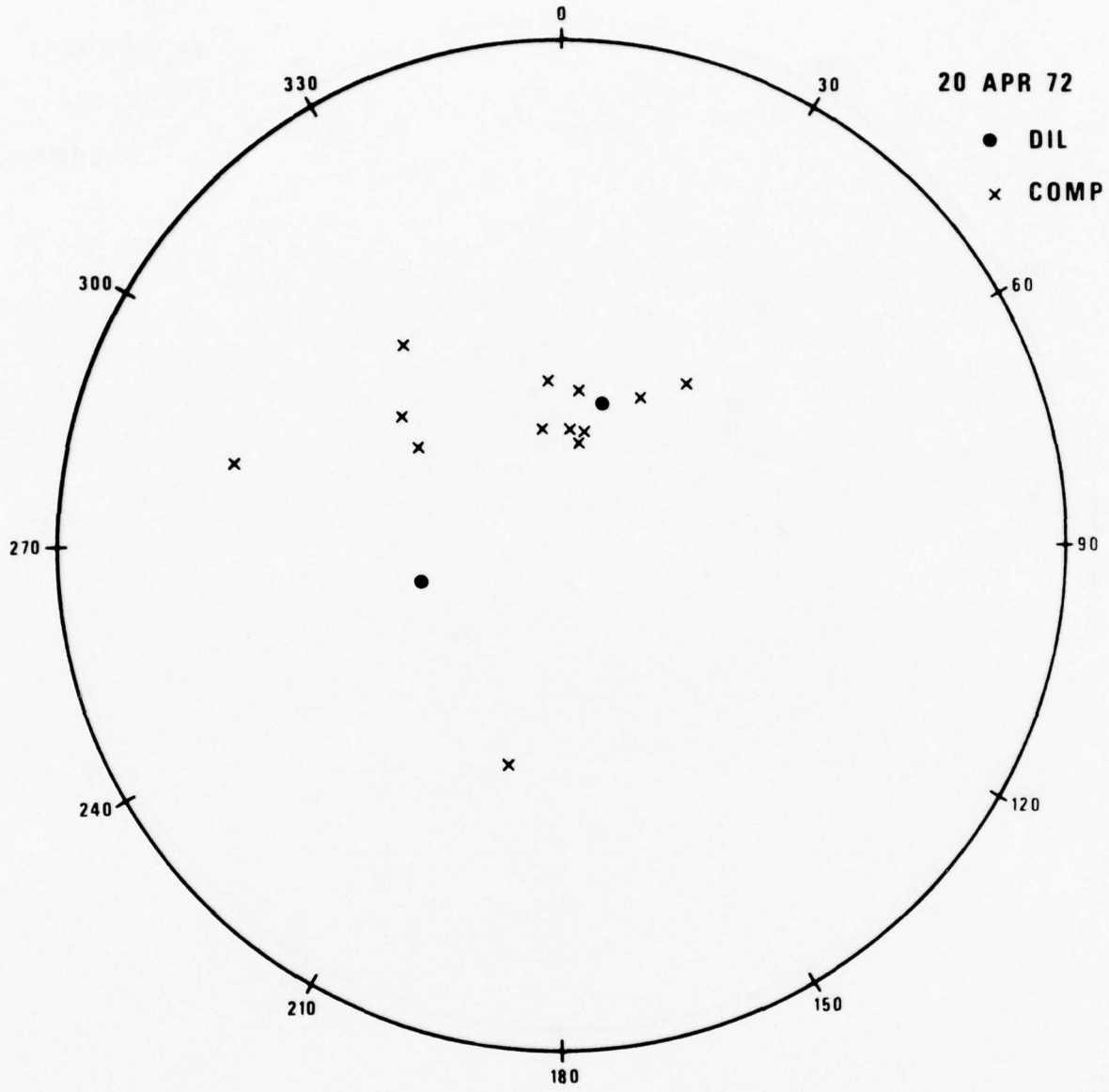

Figure 2 (Continued). First motions for Tien Shan earthquakes in the lower half of the focal sphere (Wulff net).

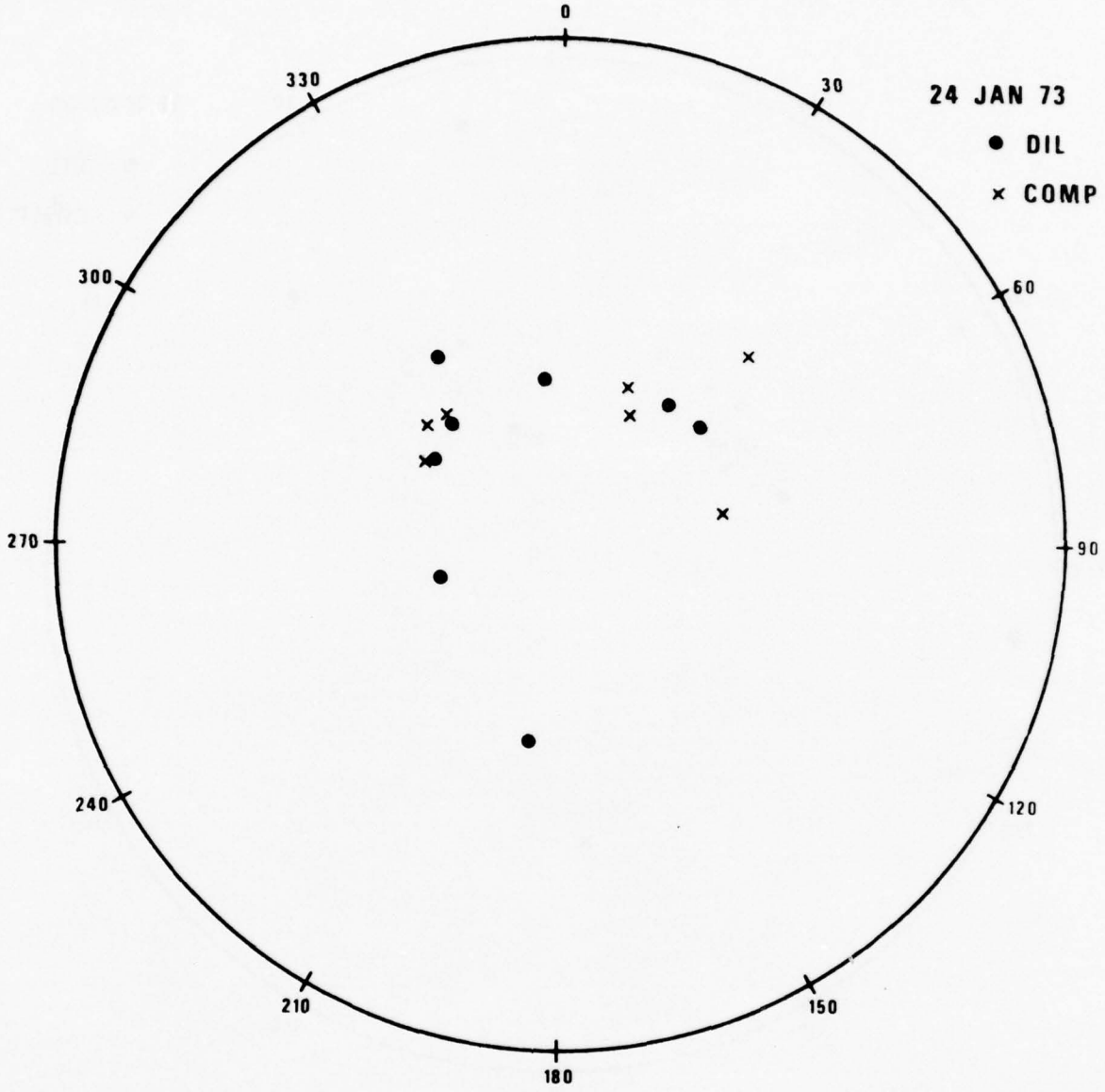

Figure 2 (Continued). First motions for Tien Shan earthquakes in the lower half of the focal sphere (Wulff net).

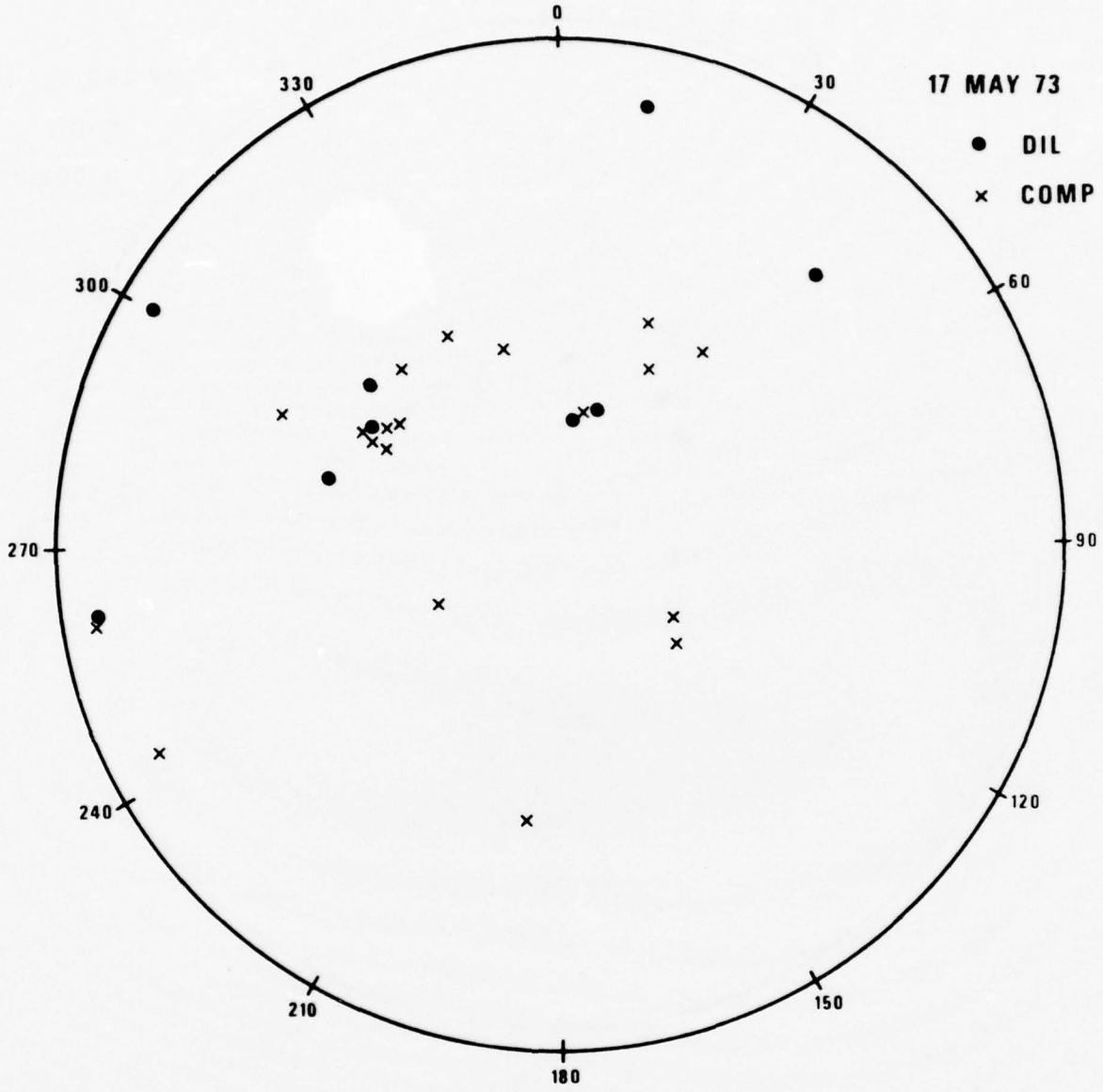

Figure 2 (Continued). First motions for Tien Shan earthquakes in the lower half of the focal sphere (Wulff net).

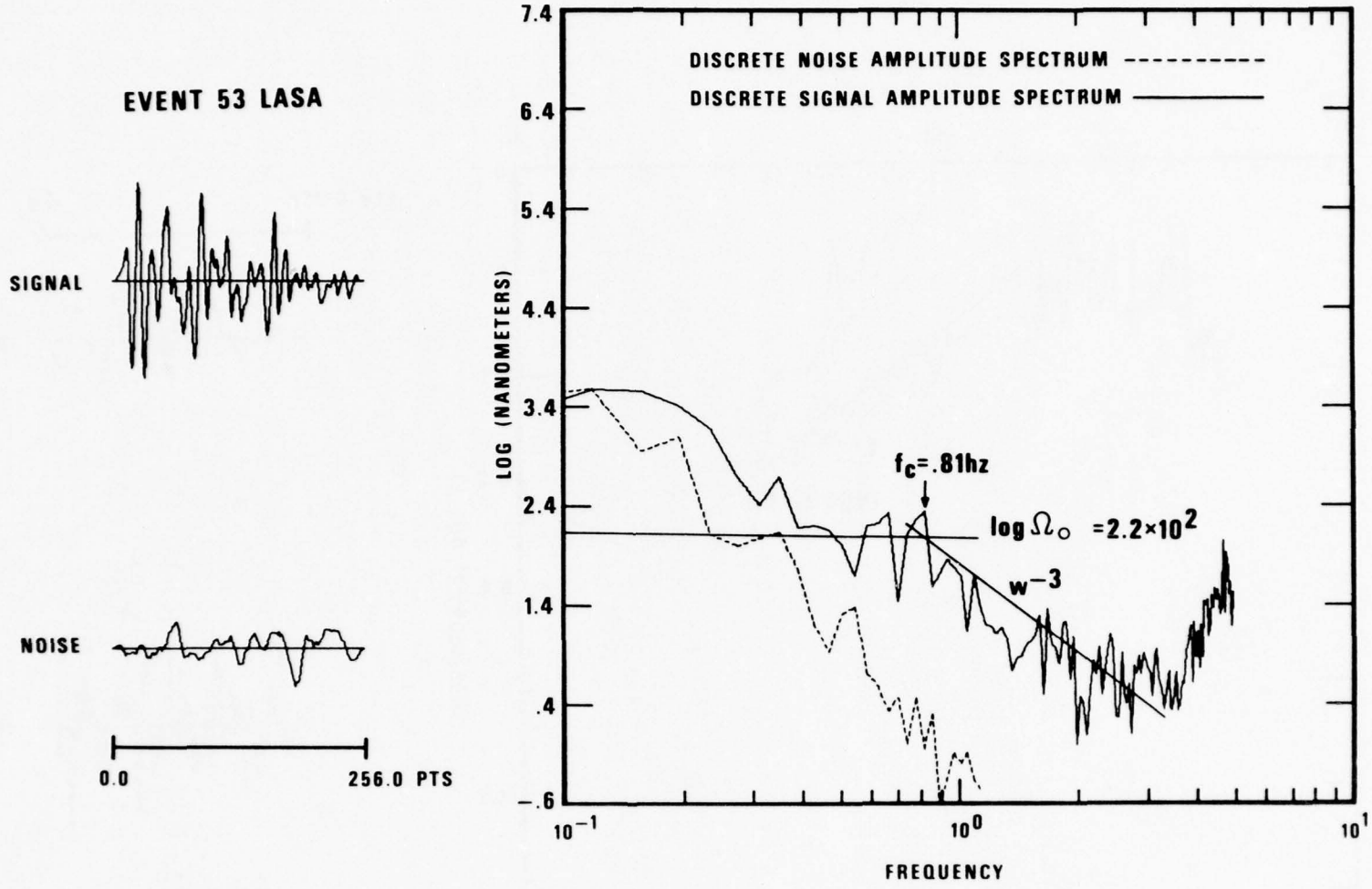

Figure 3. LASA A0 and NORSAR C3 subarray spectra of P waves from Tien Shan earthquakes with instrument response and attenuation removed.

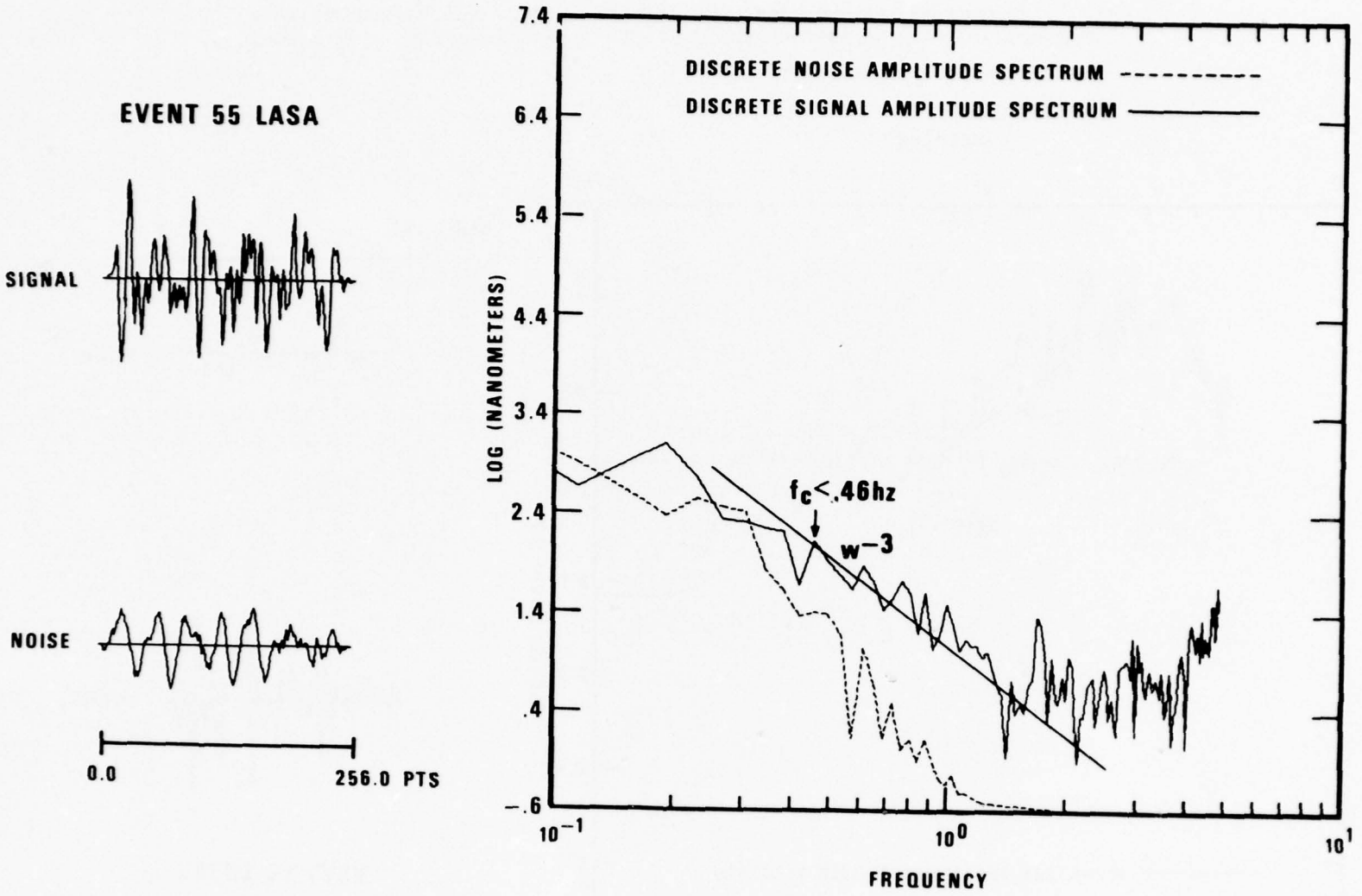

Figure 3 (Continued). LASA A0 and NORSAR C3 subarray spectra of P waves from Tien Shan earthquakes with instrument response and attenuation removed.

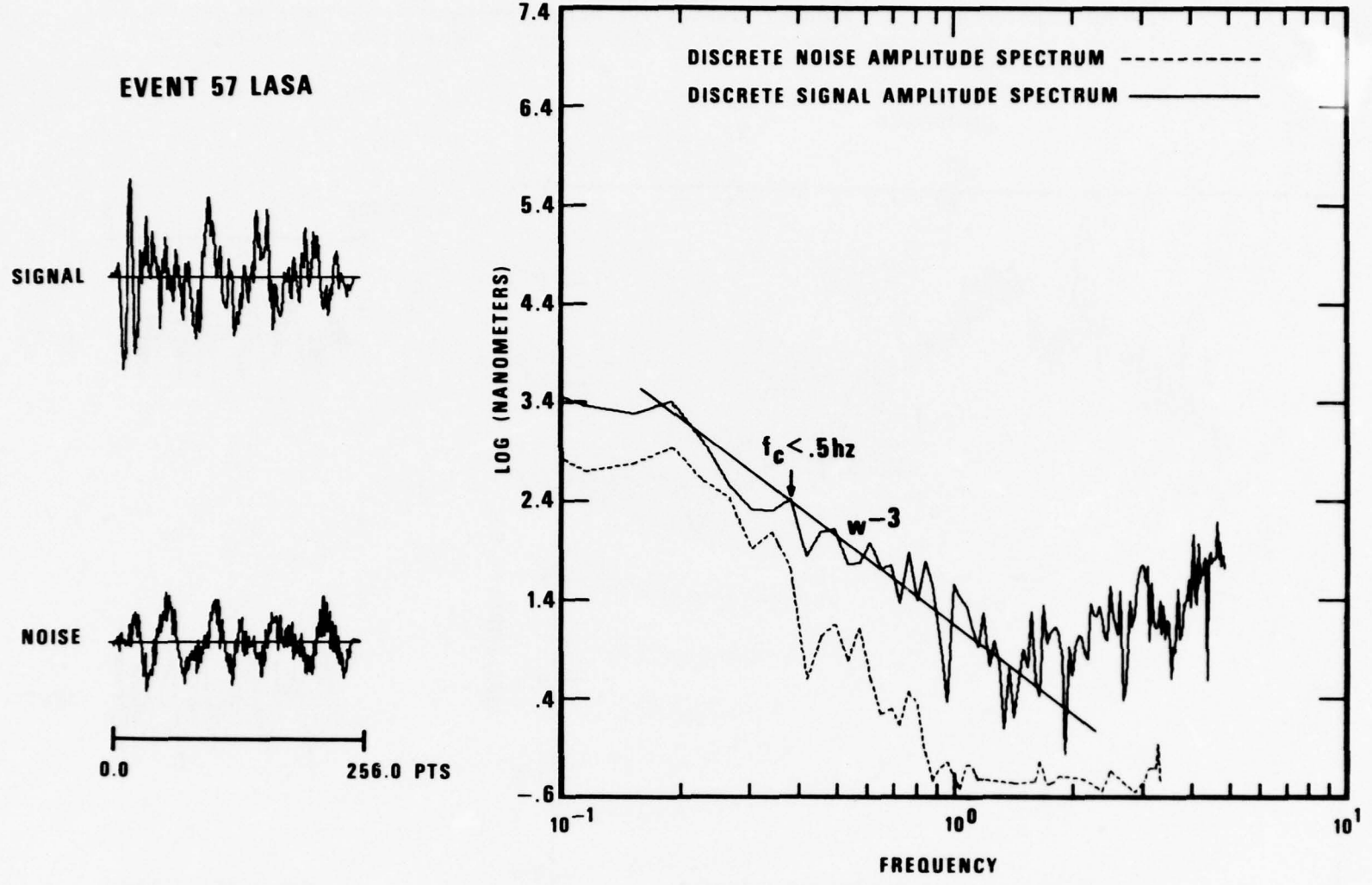

Figure 3 (Continued). LASA A0 and NORSAR C3 subarray spectra of P waves from Tien Shan earthquakes with instrument response and attenuation removed.

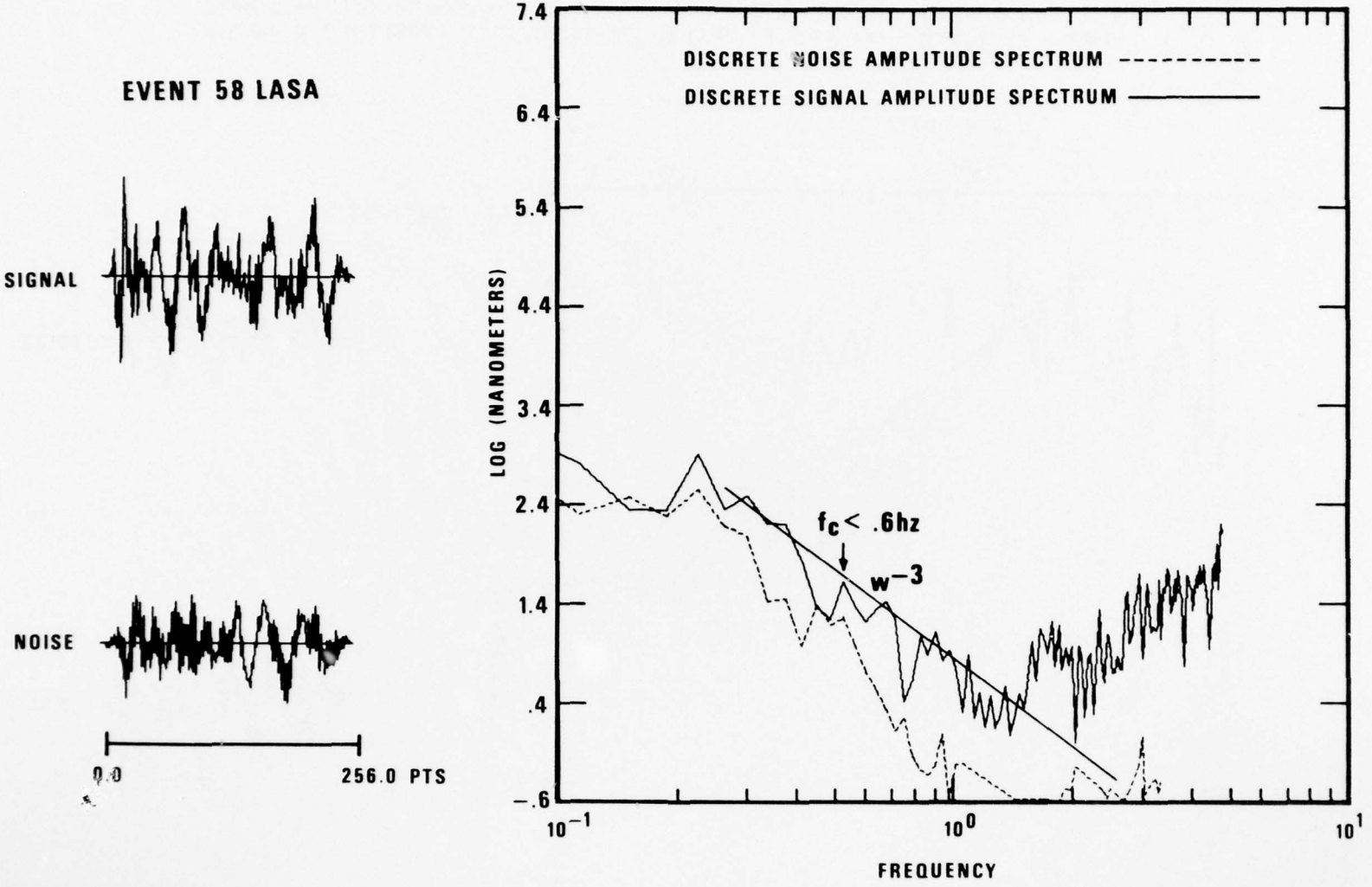

Figure 3 (Continued). LASA A0 and NORSAR C3 subarray spectra of P waves from Tien Shan earthquakes with instrument response and attenuation removed.

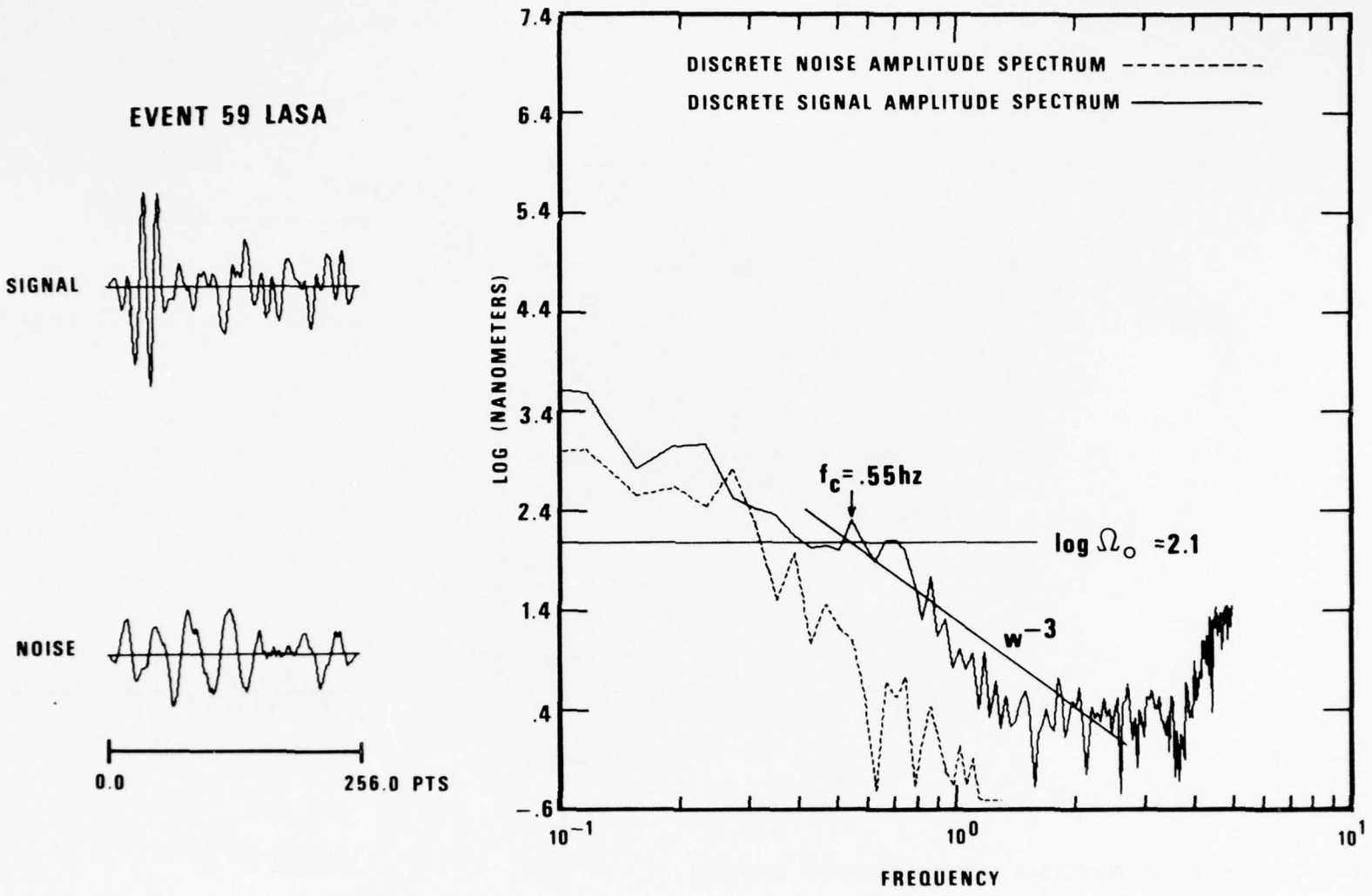

Figure 3 (Continued). LASA A0 and NORSAR C3 subarray spectra of P waves from Tien Shan earthquakes with instrument response and attenuation removed.

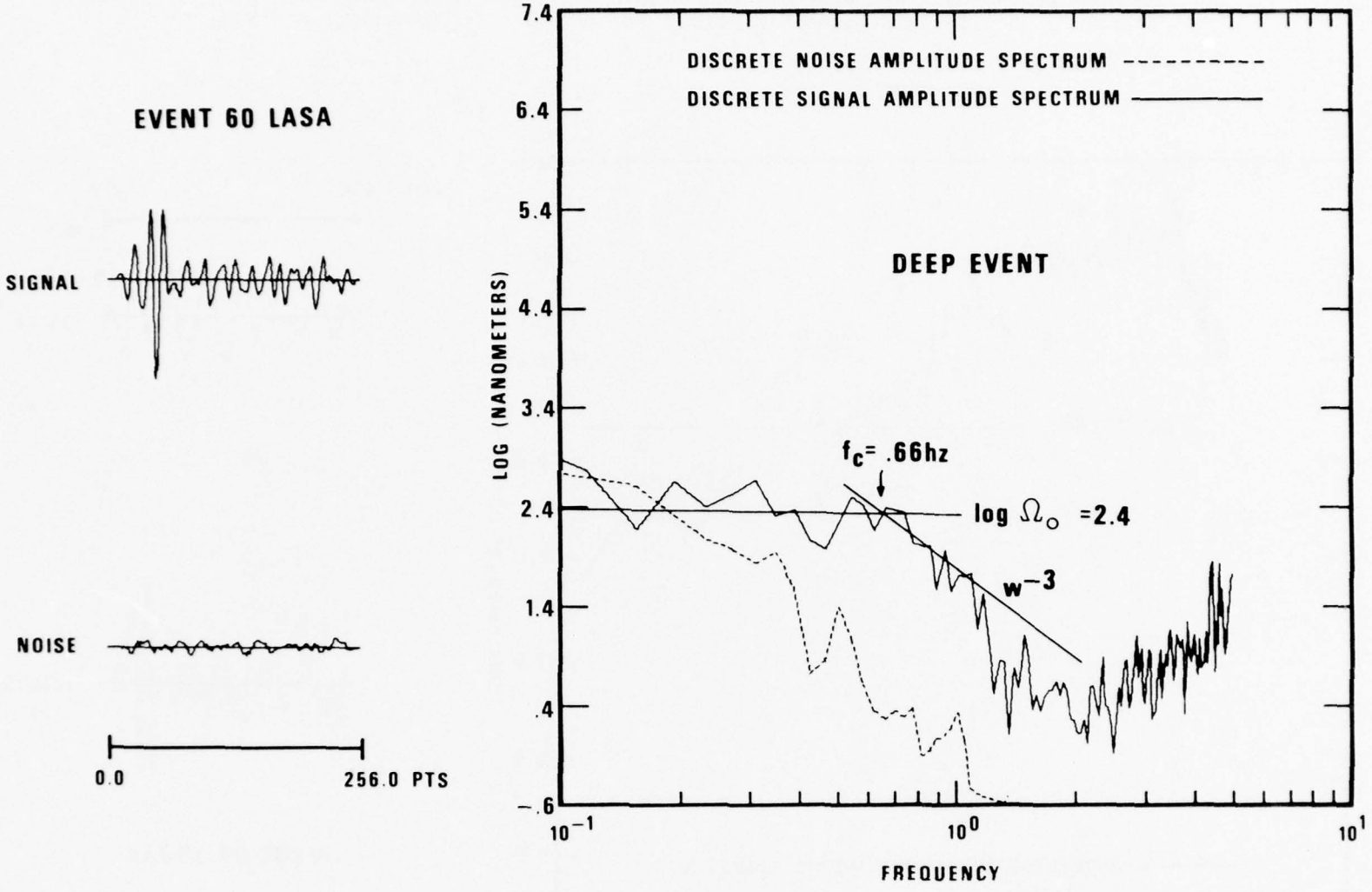

Figure 3 (Continued). LASA A0 and NORSAR C3 subarray spectra of P waves from Tien Shan earthquakes with instrument response and attenuation removed.

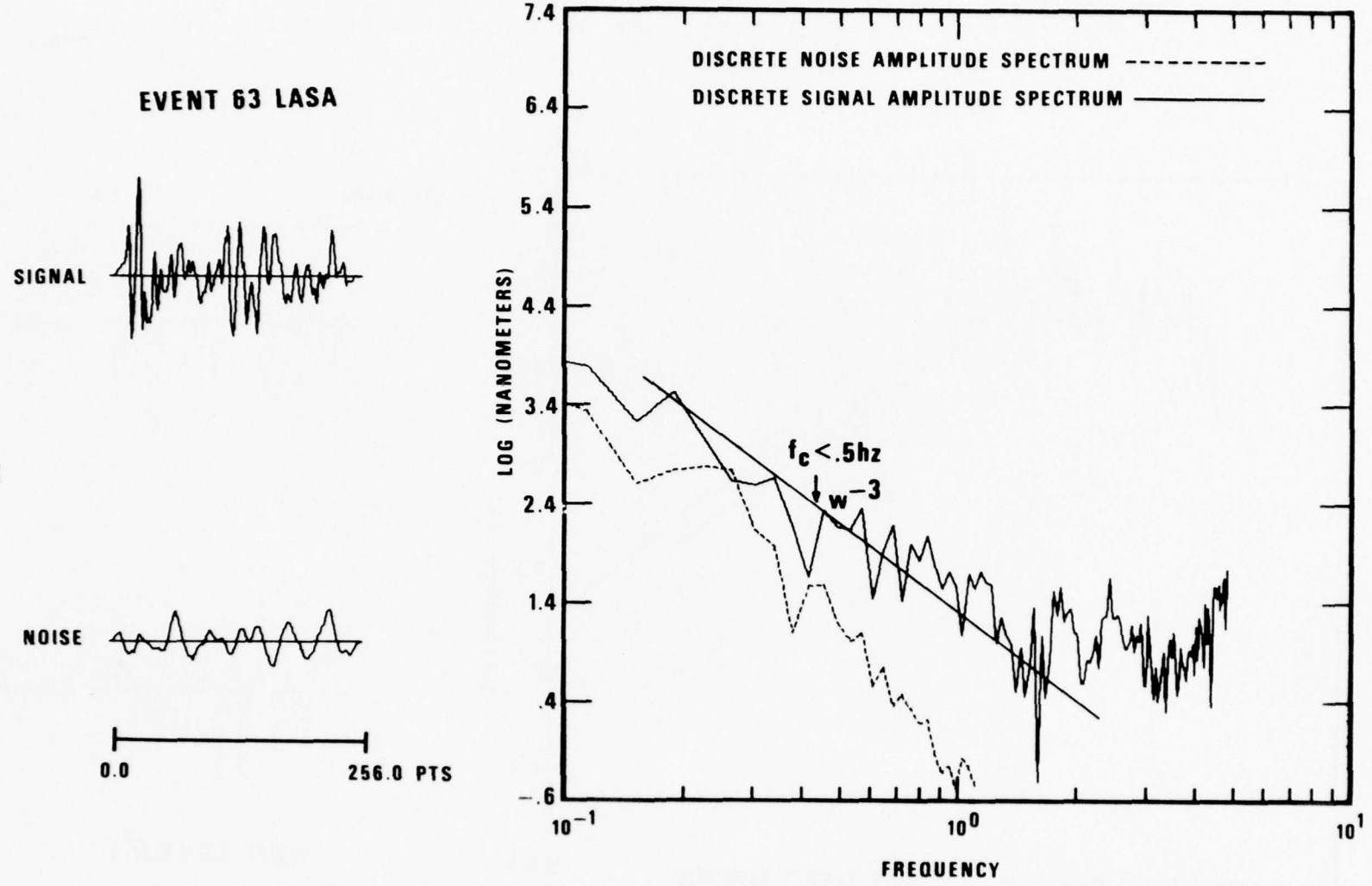

Figure 3 (Continued). LASA A0 and NORSAR C3 subarray spectra of P waves from Tien Shan earthquakes with instrument response and attenuation removed.

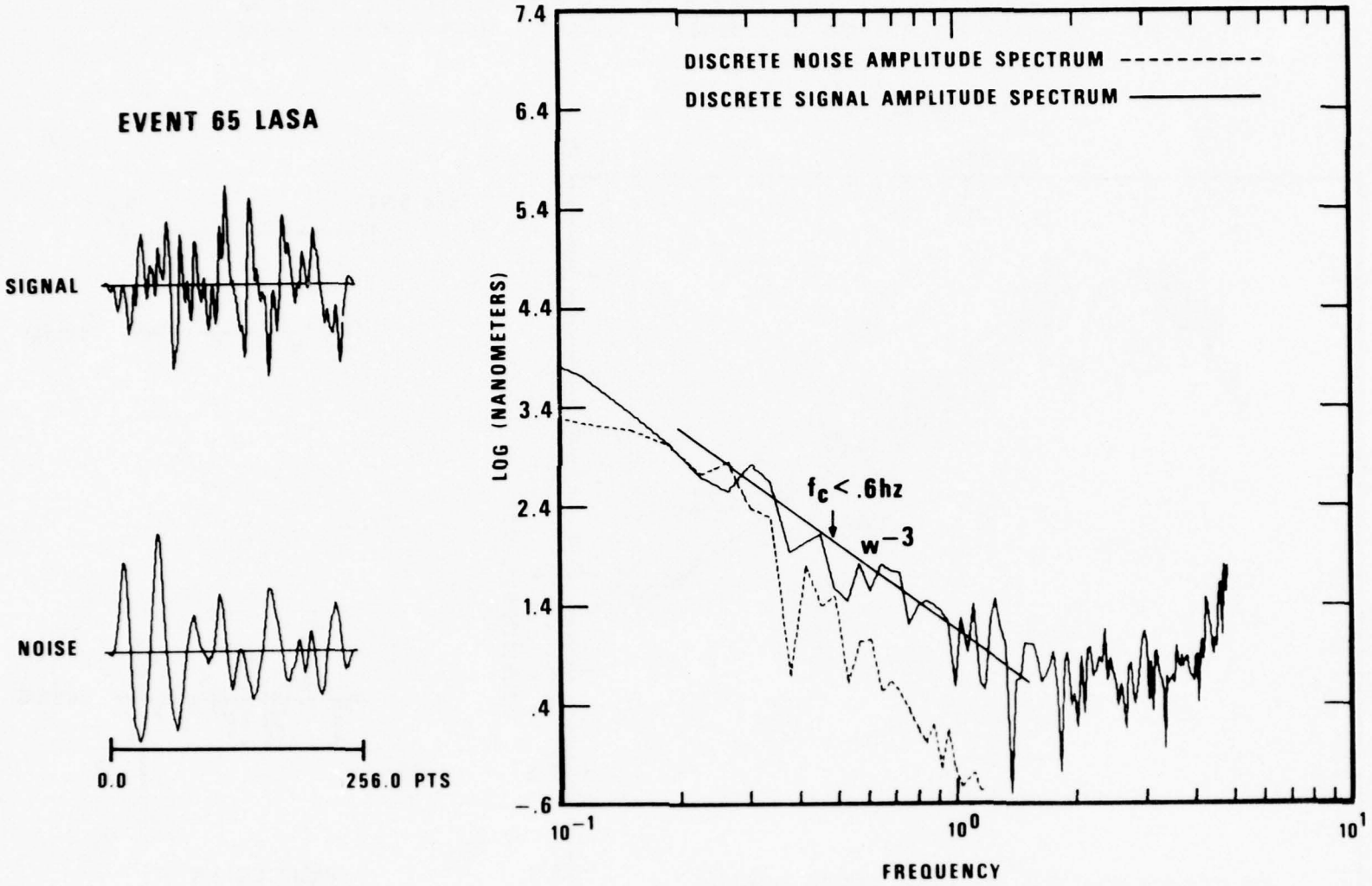

Figure 3 (Continued). LASA A0 and NORSAR C3 subarray spectra of P waves from Tien Shan earthquakes with instrument response and attenuation removed.

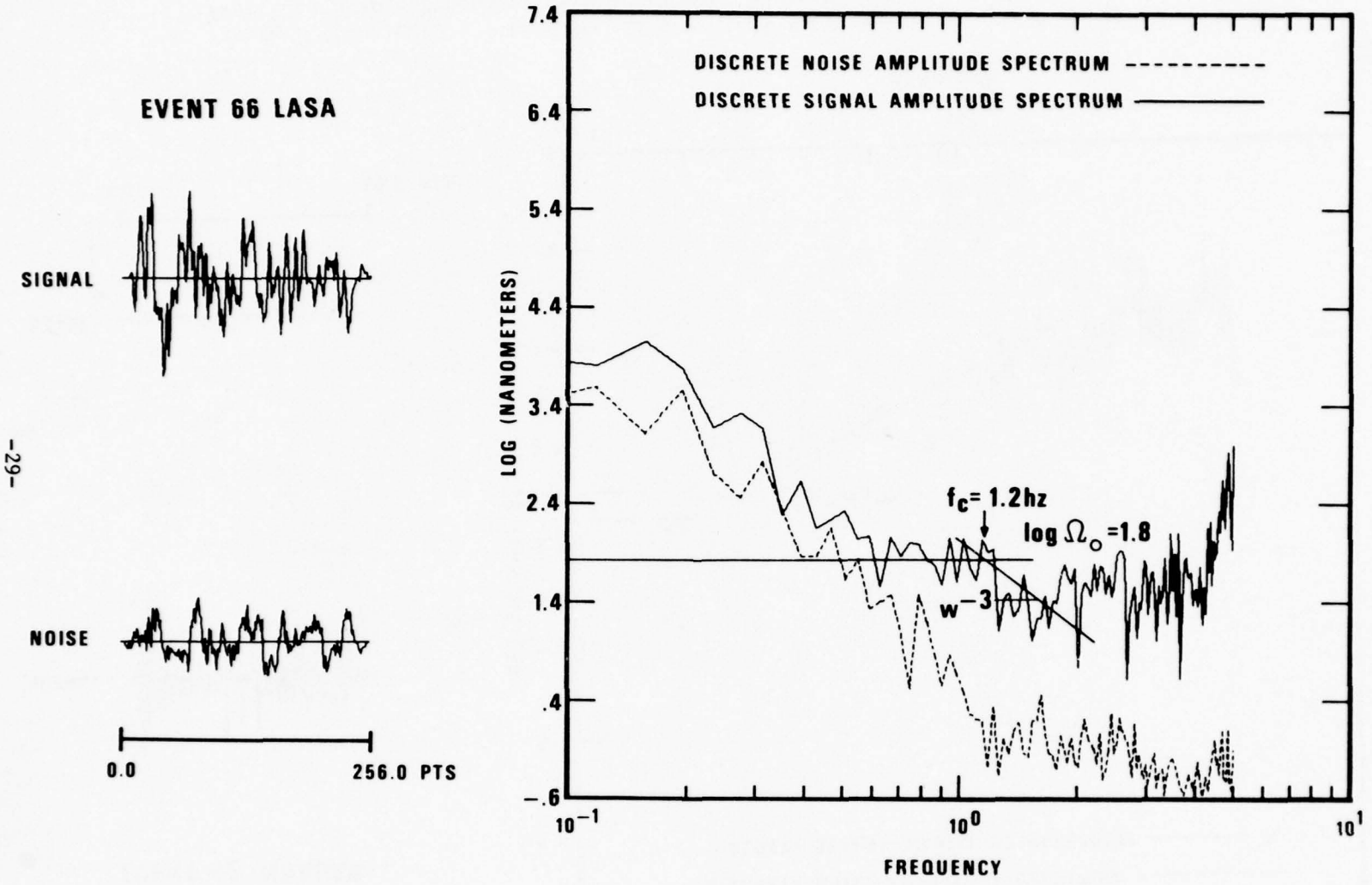

Figure 3 (Continued). LASA AO and NORSAR C3 subarray spectra of P waves from Tien Shan earthquakes with instrument response and attenuation removed.

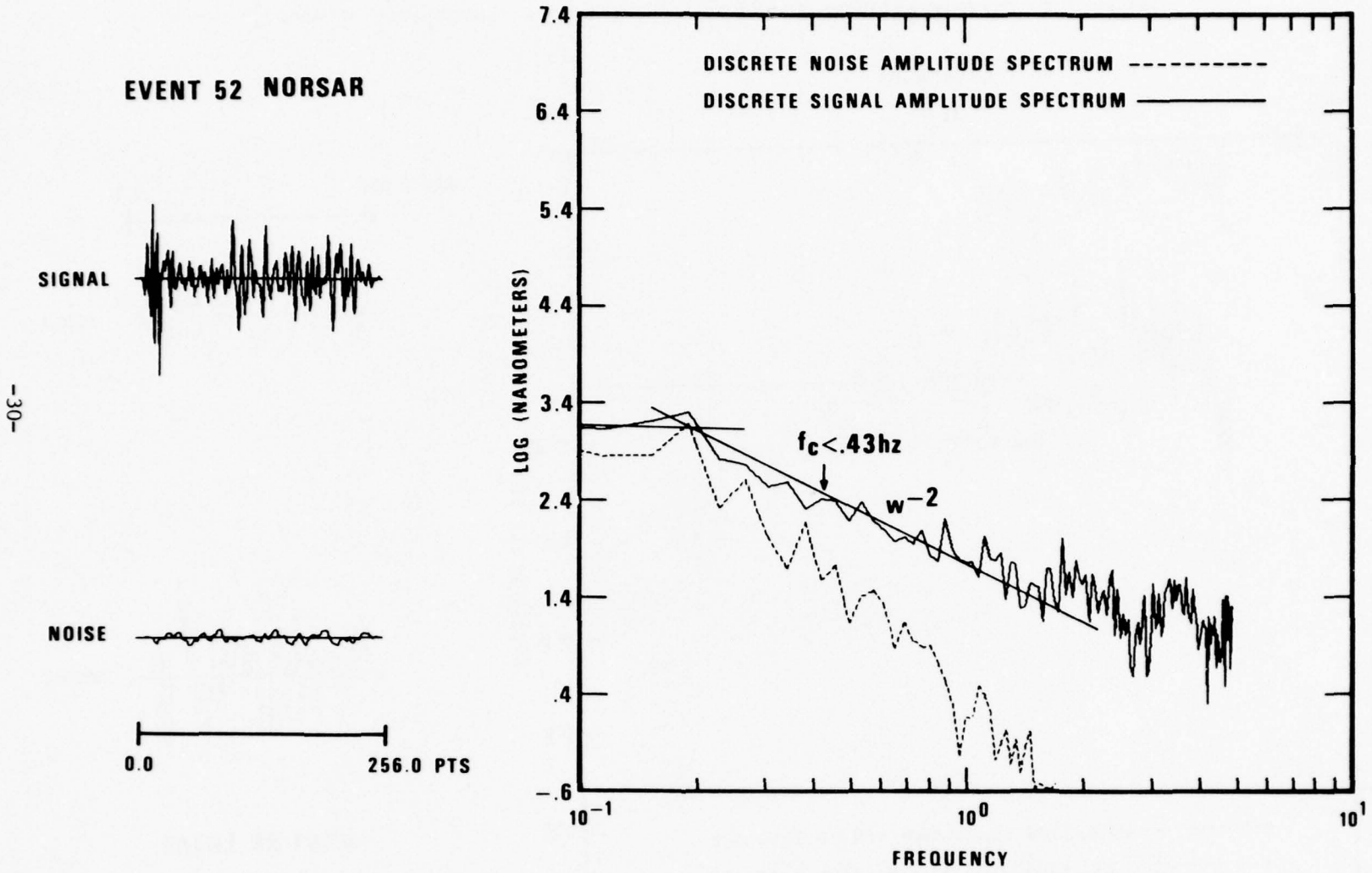

Figure 3 (Continued). LASA AO and NORSAR C3 subarray spectra of P waves from Tien Shan earthquakes with instrument response and attenuation removed.

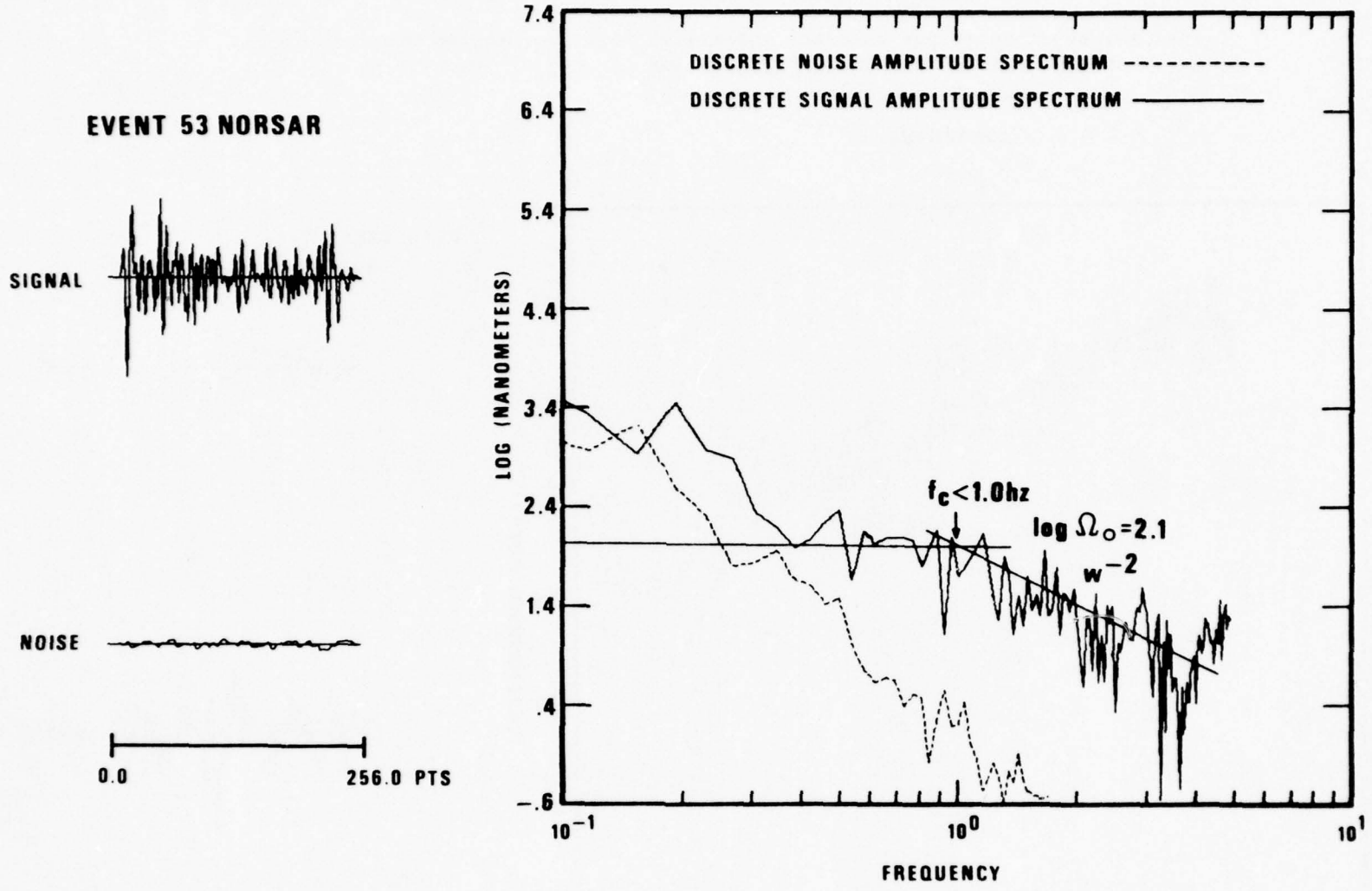

Figure 3 (Continued). LASA A0 and NORSAR C3 subarray spectra of P waves from Tien Shan earthquakes with instrument response and attenuation removed.

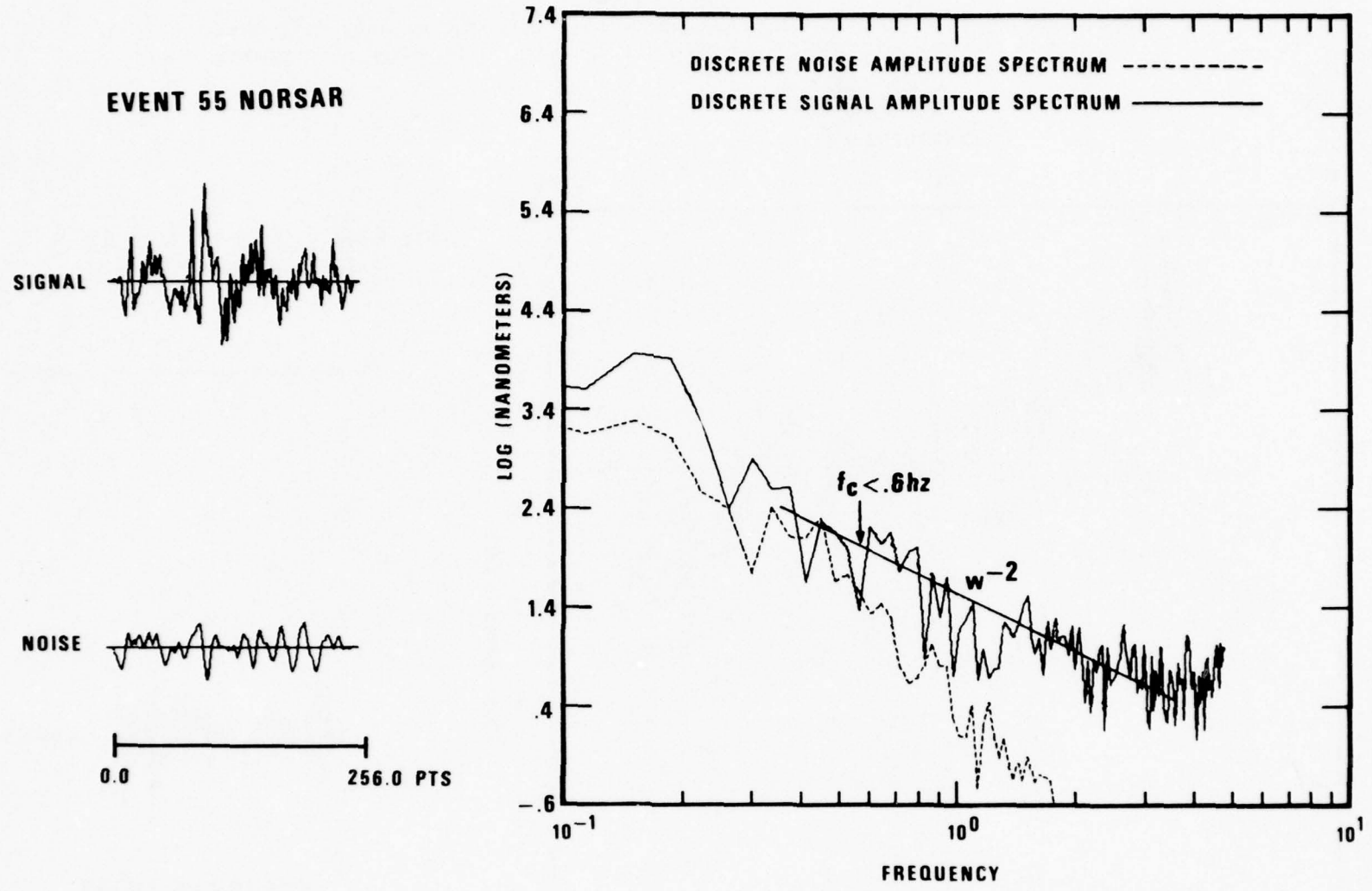

Figure 3 (Continued). LASA AO and NORSAR C3 subarray spectra of P waves from Tien Shan earthquakes with instrument response and attenuation removed.

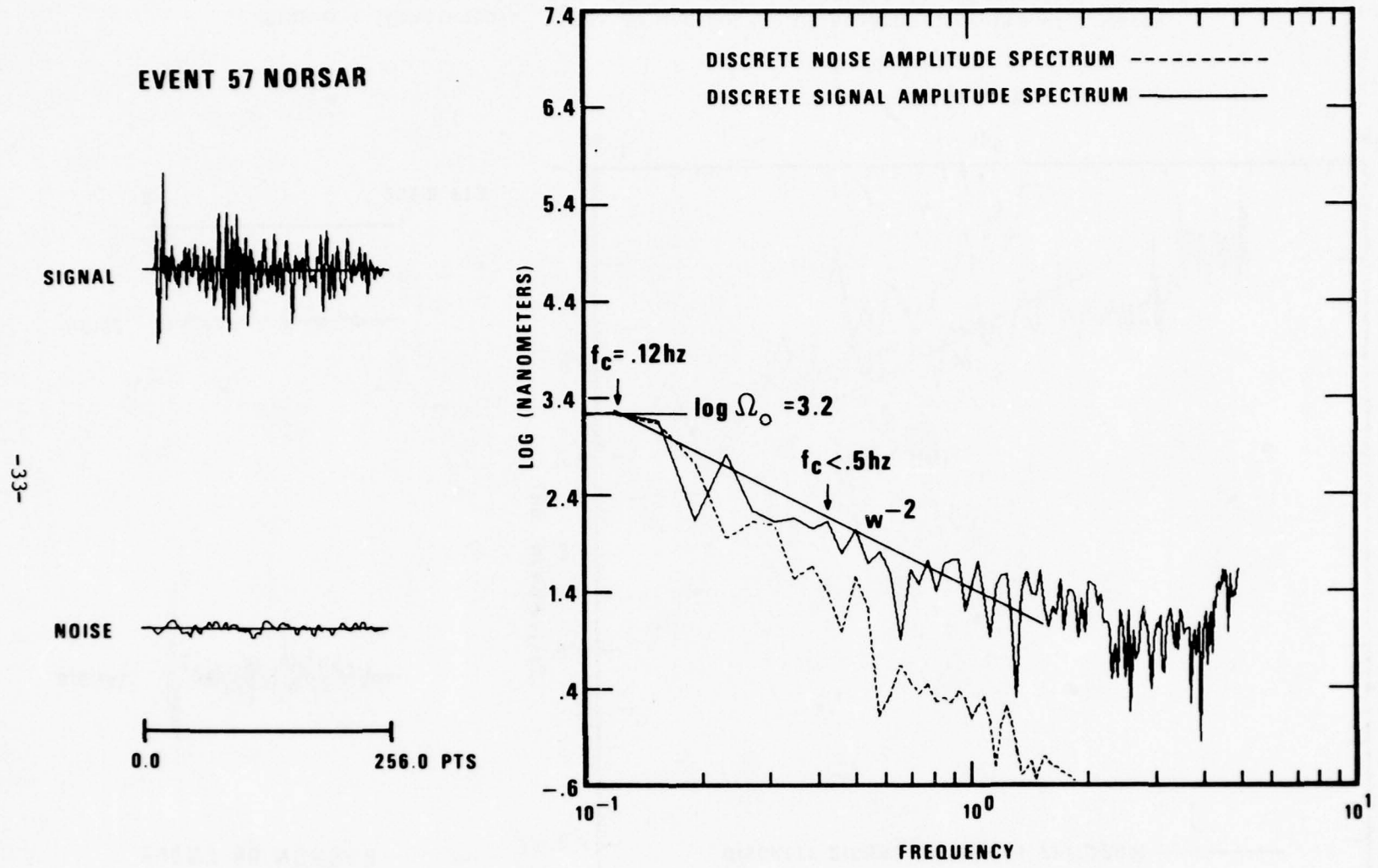

Figure 3 (Continued). LASA A0 and NORSAR C3 subarray spectra of P waves from Tien Shan earthquakes with instrument response and attenuation removed.

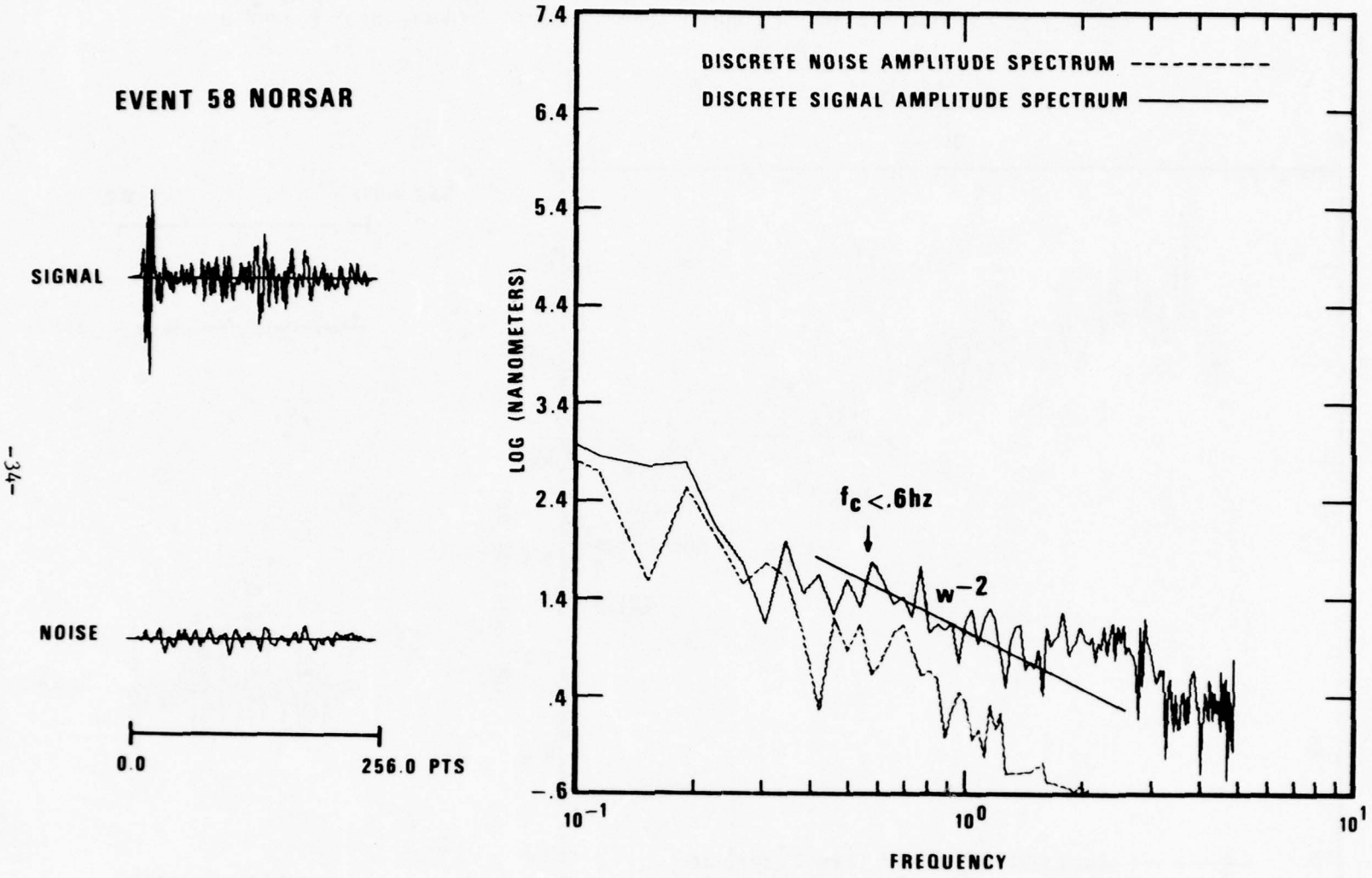

Figure 3 (Continued). LASA AO and NORSAR C3 subarray spectra of P waves from Tien Shan earthquakes with instrument response and attenuation removed.

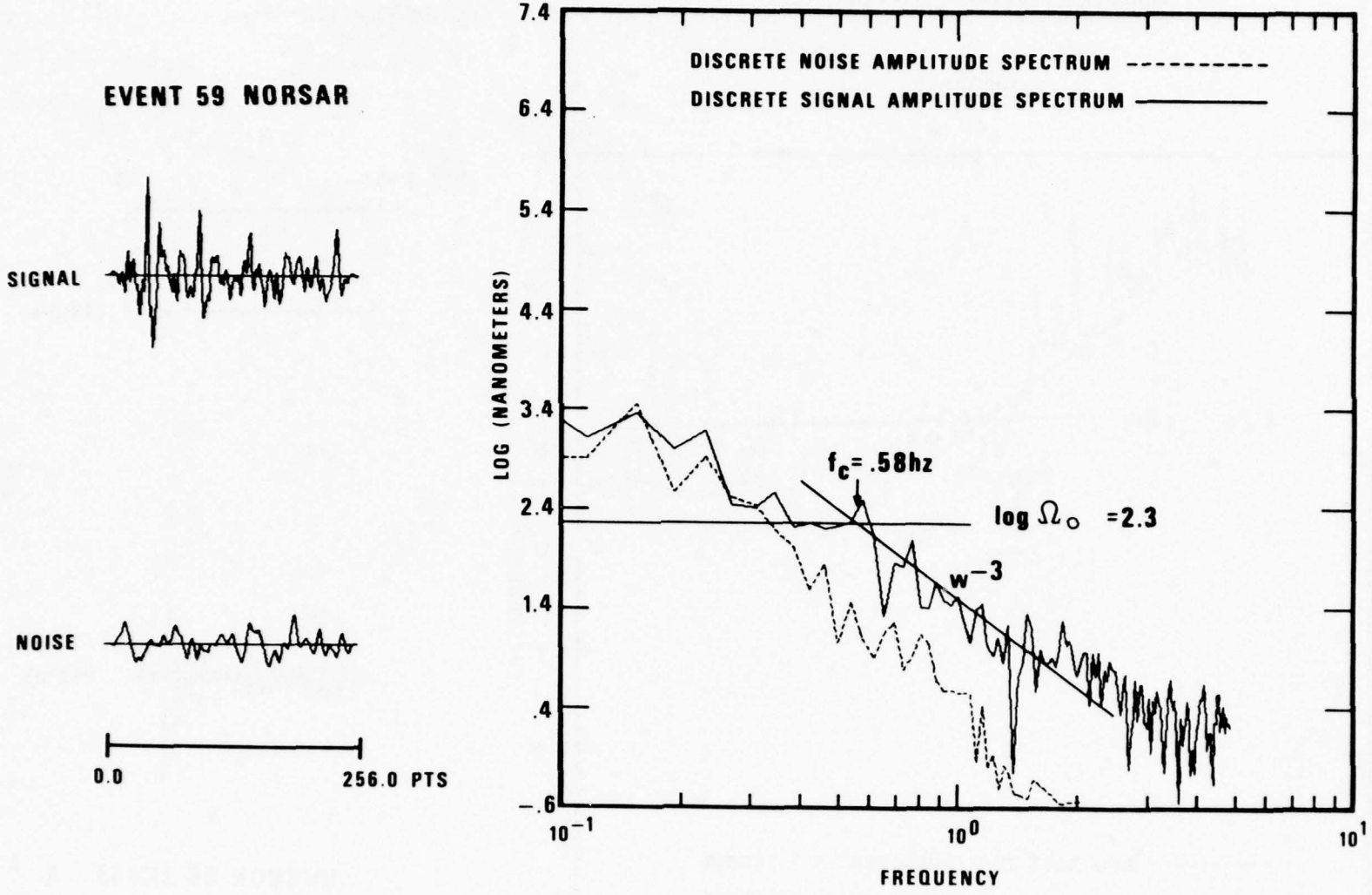

Figure 3 (Continued). LASA AO and NORSAR C3 subarray spectra of P waves from Tien Shan earthquakes with instrument response and attenuation removed.

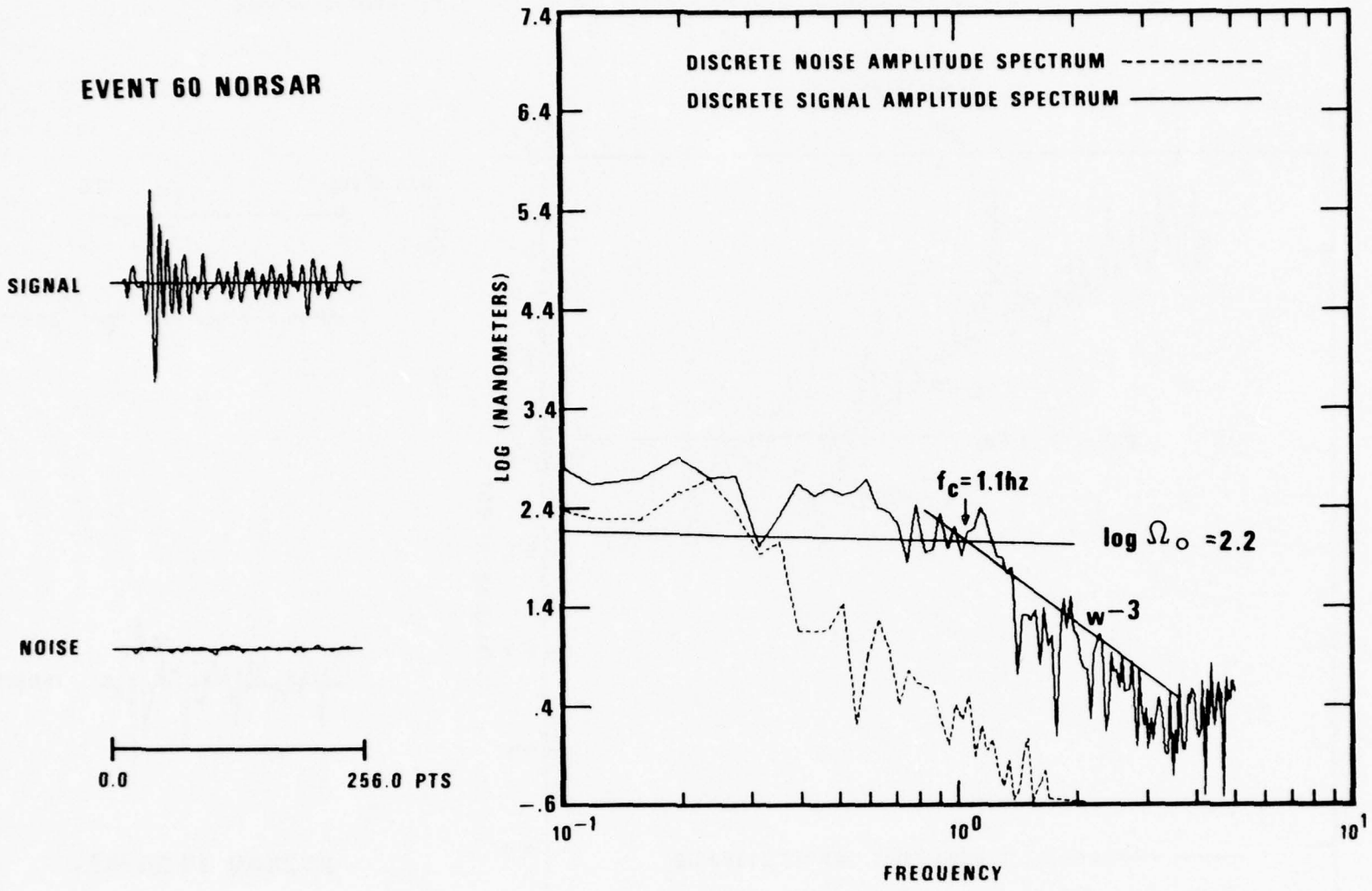

Figure 3 (Continued). LASA AO and NORSAR C3 subarray spectra of P waves from Tien Shan earthquakes with instrument response and attenuation removed.

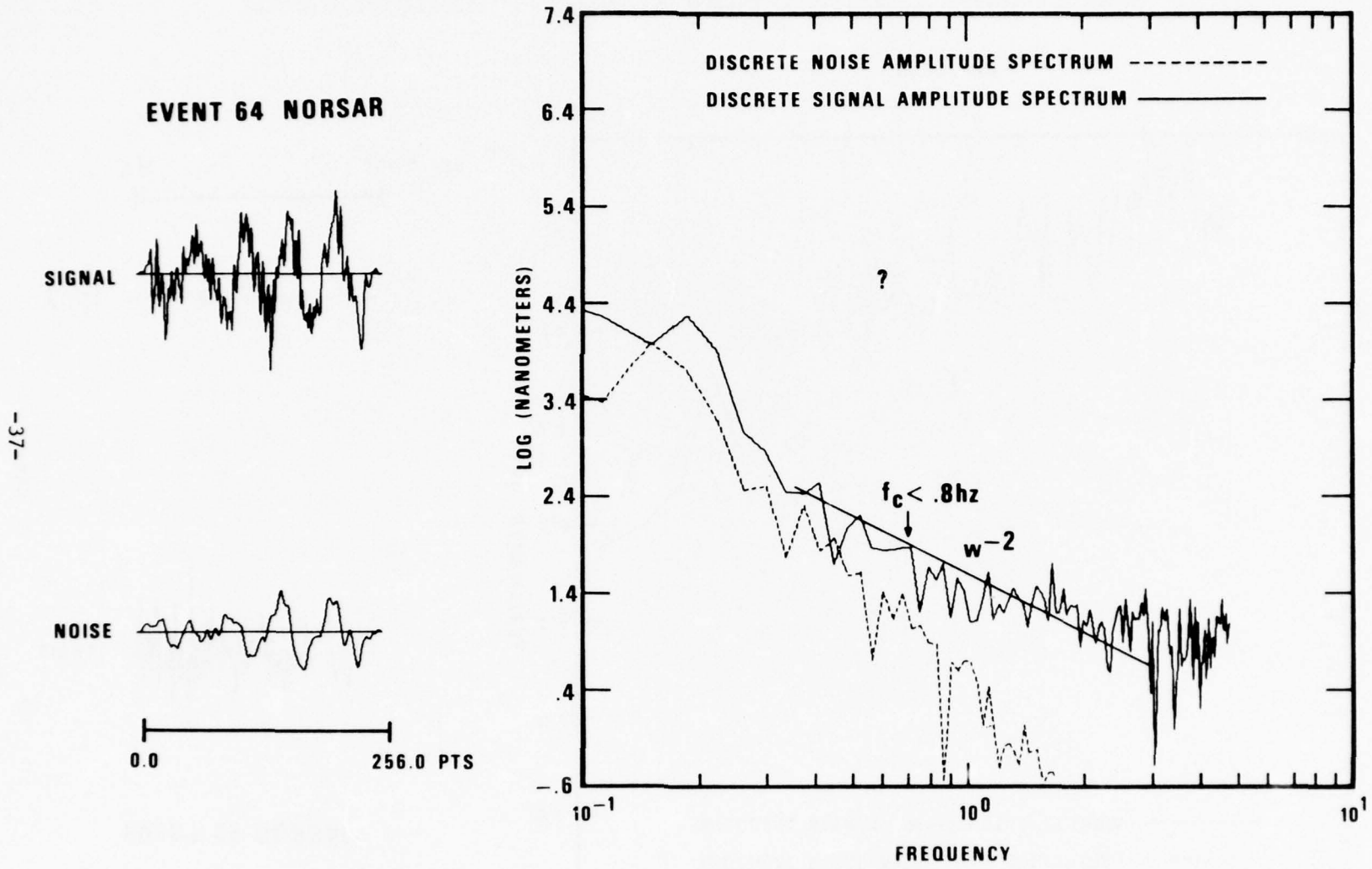

Figure 3 (Continued). LASA AO and NORSAR C3 subarray spectra of P waves from Tien Shan earthquakes with instrument response and attenuation removed.

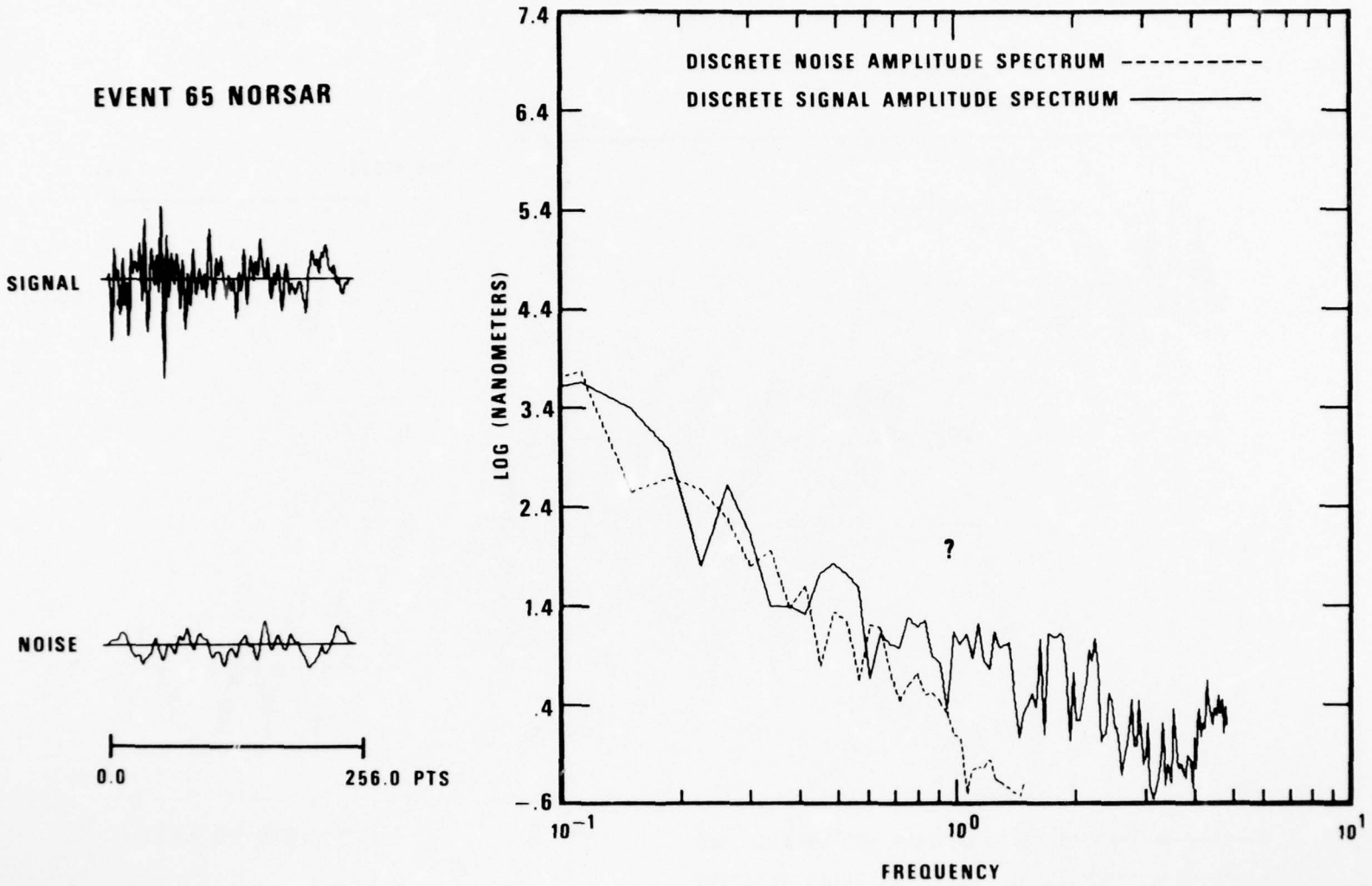

Figure 3 (Continued). LASA AO and NORSAR C3 subarray spectra of P waves from Tien Shan earthquakes with instrument response and attenuation removed.

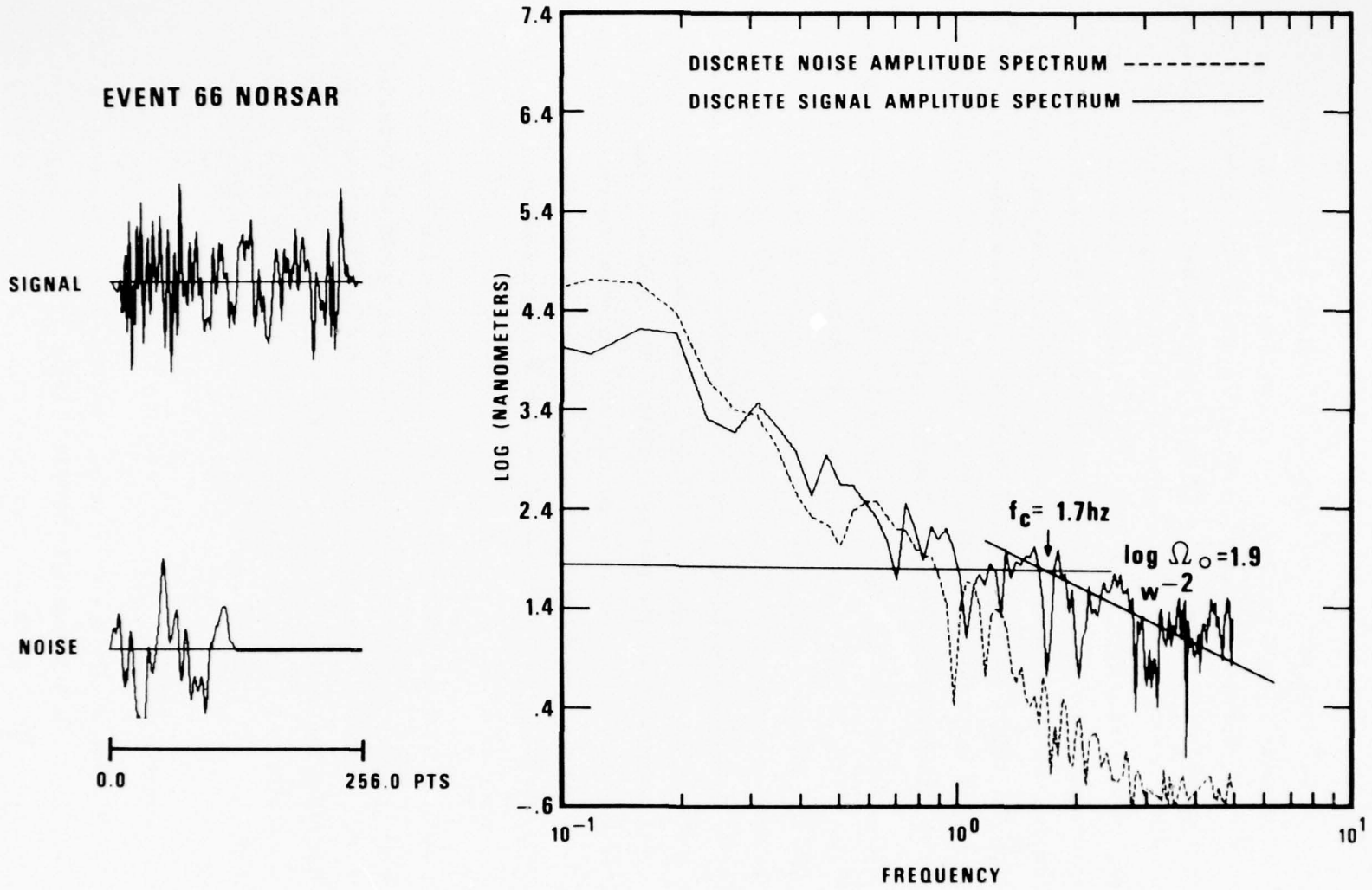

Figure 3 (Continued). LASA A0 and NORSAR C3 subarray spectra of P waves from Tien Shan earthquakes with instrument response and attenuation removed.

where $R_{\Theta\phi}$ was assumed to be unity due to lack of knowledge of the focal mechanism, values of $\rho\alpha^3$ from Table I appropriate to the source depth were used, and the divergence factor D was applied (Ben-Menahem et al., 1965). A graph of moment versus corner frequency is shown in Figure 4. Our events fall between the constant stress drop lines of Hanks and Thatcher (1972), indicating that our events are of intermediate stress drop. The average data for 4 Kazakh explosions and our event 66 fall to the right of the points. Here noise measurements were used as upper bounds for the signal amplitude in several cases; the arrows indicate that the data would have lower corner frequencies and higher moments if the background noise had been less. One expects that for the same moment, explosions will have higher corner frequencies than earthquakes (Hanks and Thatcher, 1972).

We attempted to find the LR radiation pattern for each event by plotting the antilogs of the M_s values for each event, as listed in Table III. The results for the largest earthquake, event 60, are shown in Figure 5. The data point with an arrow is a noise measurement. The observed distribution of amplitudes does not readily conform to any quadripole radiation pattern, which is probably due to propagation effects, the large epicentral distances, and the small magnitudes of the events studies. The scatter of data points was so poor that no attempt was made to find the best-fitting radiation patterns. By comparison, von Seggern and Sobel (1976) show distributions of LR amplitudes which indicate thrust mechanisms for a set of Kamchatka events.

Propagation Effects

We measured relative mantle attenuation along the paths from the Tien Shan to LASA and NORSAR, the only two sites for which we had short-period digital data. Our measurement of attenuation is the factor t*, which is the travel time along the ray path divided by the average attenuation factor Q. Knowing t* for one ray path, one can find t* for a second ray path by finding the ratio of spectra of common events for the two paths according to the expression

$$m = - \pi(t_1^* - t_2^*)$$

where m is the slope of the spectral ratio. Noponen (1975) reports a t* of .20 for paths from Eastern Kazakh to NORSAR. Figure 6 shows the ratio of the average spectra of the Tien Shan events recorded at NORSAR divided by the

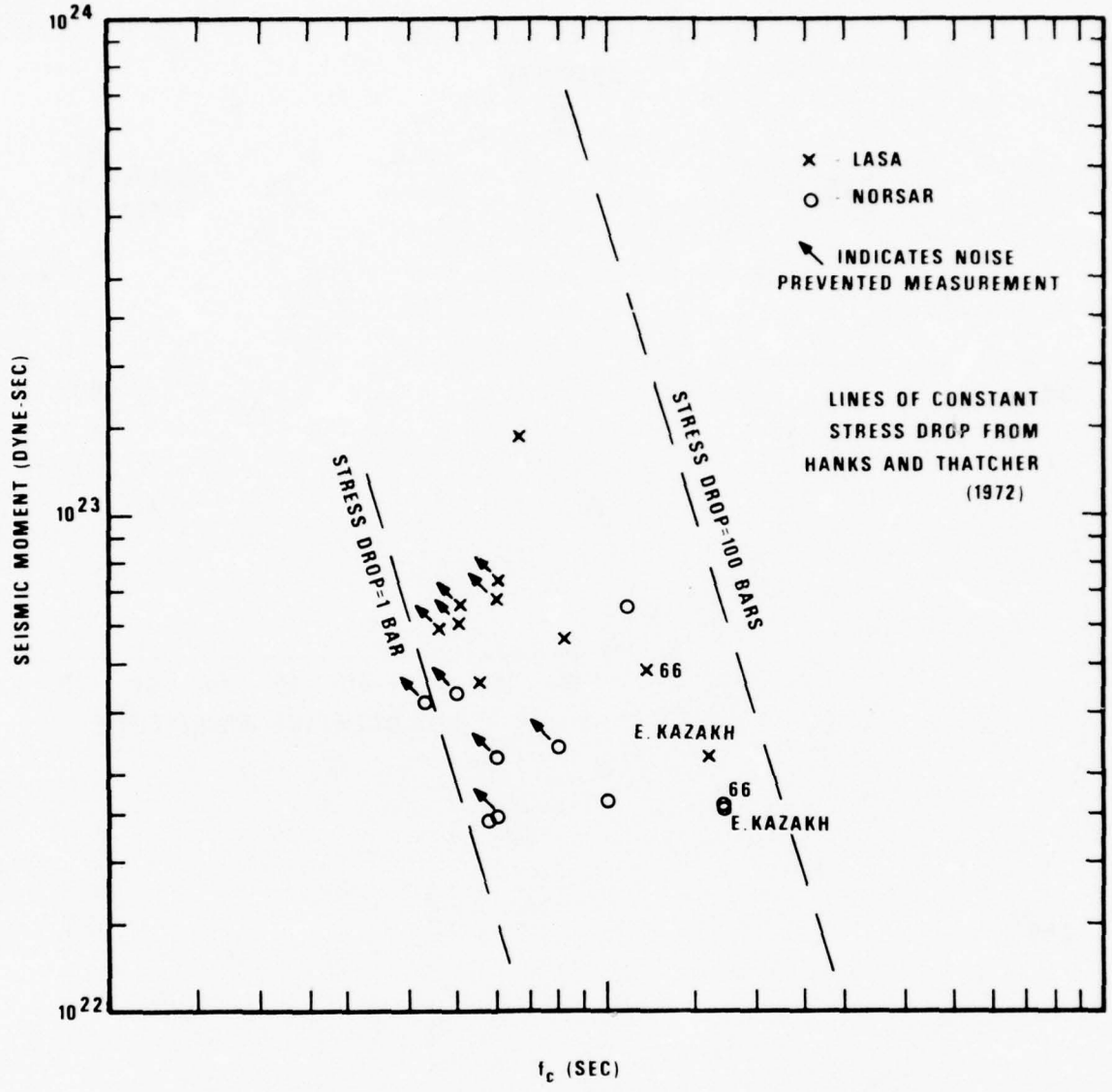

Figure 4. Seismic moment versus corner frequency for Tien Shan earthquakes from LASA and NORSAR P recordings.

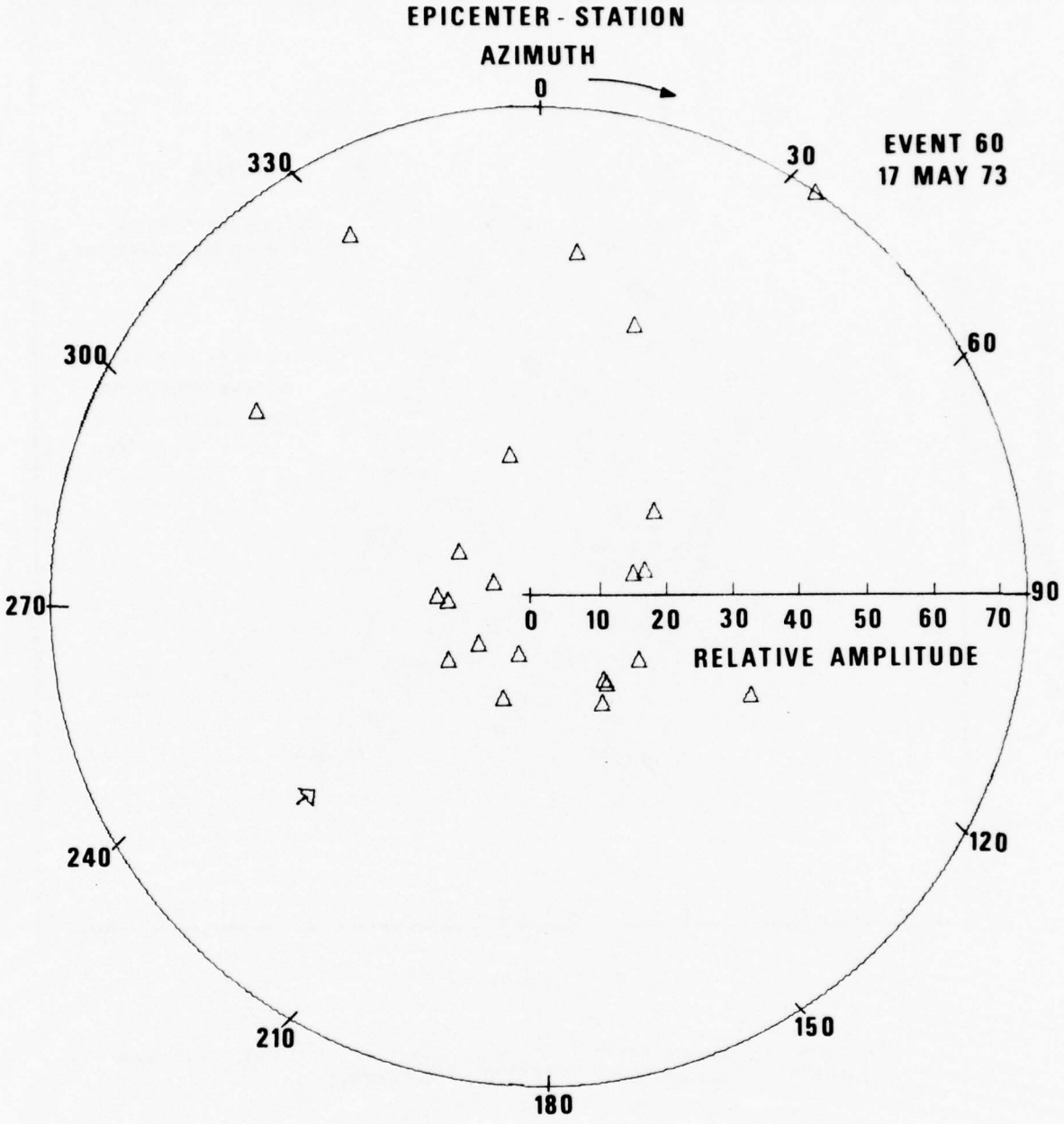

Figure 5. Observed LR amplitudes (T=20 sec) for Tien Shan earthquakes of this study.

TABLE III

MAGNITUDE DATA FOR TIEN SHAN EARTHQUAKES

EVENT = 52

STATION	DELTA	m_b	STATION	DELTA	M_s
BUL	82.10	4.31	BUL	82.10	-4.69
GDH	62.96	-5.38	GDH	62.96	-5.41
HKC	32.35	-5.30	IST	40.73	4.19
HLW	44.44	-4.99	KEV	38.53	4.85
IST	40.73	4.73	MAT	40.63	4.49
JER	40.62	4.98	NAI	62.30	4.49
KEV	38.53	4.88	NDI	16.56	4.87
OGD	93.32	-5.12	NOR	48.42	-4.61
MAT	40.63	4.16	POO	27.12	4.97
NAI	62.30	-4.97	QUE	19.93	4.35
NDI	16.56	4.20	SHI	29.52	4.43
NOR	48.42	4.53	SHK	37.61	4.43
POO	27.12	4.63	ALO	101.00	4.77
QUE	19.93	4.18	CHG	27.76	4.64
SEO	32.11	-4.40	COL	63.85	5.06
SHI	29.52	4.60	KIP	93.03	-5.69
SHL	19.25	4.52	OGD	93.32	-4.79
STU	50.50	4.66	CHG	27.76	4.62
SHK	37.61	4.47	CTA	84.84	4.02
SNG	39.17	4.66	EIL	42.01	4.21
ALQ	101.00	4.43	KON	46.45	4.80
CHG	27.76	4.56	OGD	93.32	5.02
COL	63.85	-6.21	TLO	63.17	4.28
EIL	42.01	-4.71			
KIP	93.03	-6.20			
KON	46.45	5.12			
AVERAGE		4.54			4.56

- minus sign by magnitude means it is an upper limit based on noise measurement since signal was not observed

TABLE III (Continued)

MAGNITUDE DATA FOR TIEN SHAN EARTHQUAKES

EVENT = 53

STATION	DELTA	m_b	STATION	DELTA	M_s
BUL	80.39	4.40	BUL	80.39	-4.38
GDH	65.01	4.96	GDH	65.01	-5.04
HKC	31.57	5.26	HKC	31.57	4.25
IST	41.00	5.24	IST	41.00	-3.59
JER	40.23	4.72	JER	40.23	-3.88
KEV	40.32	5.00	KEV	40.32	-4.58
MAT	41.42	4.47	MAT	41.42	-4.20
MSH	20.06	-5.04	MSH	20.06	3.63
NAI	60.74	5.00	NAI	60.74	-4.18
NDI	14.36	5.65	QUE	18.27	3.53
NOR	40.27	4.93	SHI	28.47	-3.63
POO	24.90	5.41	SNG	37.34	3.90
WUE	18.27	4.36	ALQ	103.00	-5.03
SEO	32.73	4.90	COL	65.80	4.85
SHI	28.47	4.27	EIL	41.52	-3.90
SHL	17.30	4.87	OGD	95.37	-5.04
STU	51.42	5.18	TOL	64.00	-4.21
UME	42.33	4.86	ALQ	103.00	4.87
SNG	37.34	5.40	CHG	26.06	3.89
SHK	38.18	4.91	CTA	83.94	4.29
ALQ	103.00	4.56	FBK	66.00	2.53
CHG	26.06	4.64	OGD	95.37	4.33
COL	65.80	5.40	TLO	63.95	4.11
EIL	41.52	4.88			
OGD	95.37	-5.59			
TOL	64.00	5.75			
AVERAGE		4.95			3.91

- minus sign by magnitude means it is an upper limit based on noise measurement since signal was not observed

TABLE III (Continued)

MAGNITUDE DATA FOR TIEN SHAN EARTHQUAKES

EVENT = 55

STATION	DELTA	m_b	STATION	DELTA	M_s
ASP	79.01	4.74	EIL	43.72	-3.94
EIL	43.72	5.08	MSH	22.39	3.80
MSH	22.39	-4.97	NDI	16.45	4.21
NDI	16.45	4.69	NOR	49.83	-4.73
NOR	49.83	4.54	NUR	40.88	-4.73
NUR	40.88	4.79	POO	26.92	4.36
POO	26.92	4.49	QUE	20.74	4.21
QUE	20.74	4.50	SHI	52.55	-4.37
SEO	30.30	4.68	UME	42.60	-4.85
SHI	30.89	-4.81	SHK	35.92	4.15
SHL	17.71	4.57	BUL	82.83	-4.70
STU	52.55	5.00	GDH	64.47	-5.39
SHK	35.92	4.64	HKC	30.29	4.35
SNG	37.47	4.90	HLW	46.21	-3.68
BUL	82.83	4.51	IST	42.72	-3.62
GDH	64.47	4.67	JER	42.38	-3.61
HKC	30.29	-5.06	MAT	39.07	4.40
HLW	46.21	-5.39	ALQ	101.00	-4.54
TST	42.72	5.07	CHG	25.98	3.56
JER	42.38	4.77	COL	64.19	4.22
NIL	14.48	5.43	KIP	92.16	-5.92
MAT	39.07	4.28	KON	48.43	-4.86
ALQ	101.00	4.57	OGD	94.82	-4.50
CHG	25.98	5.14	ALQ	101.00	4.37
COL	64.19	5.00	CHG	25.98	3.57
KIP	92.16	-6.63	CTA	82.79	4.12
KON	48.43	-5.60	KIP	92.16	3.89
OGD	94.82	-5.70	KON	48.43	4.31
			OGD	94.82	4.71
			TLO	65.23	3.89
AVERAGE		4.75			4.01

- minus sign by magnitude means it is an upper limit based on noise measurement since signal was not observed

TABLE III (Continued)

MAGNITUDE DATA FOR TIEN SHAN EARTHQUAKES

EVENT = 57

STATION	DELTA	m_b	STATION	DELTA	M_s
ASP	79.80	4.44	UME	42.21	-4.49
UME	42.21	5.02	STU	51.37	-4.36
STU	51.37	4.82	SHL	17.47	4.13
SHL	17.47	4.76	SHI	28.61	3.81
SHI	28.61	-4.03	QUE	18.45	3.71
SEO	32.62	-5.18	POO	25.12	4.09
QUE	18.45	3.68	NUR	40.17	4.43
POO	25.12	4.62	NOR	50.35	4.42
NUR	40.17	4.85	NDI	14.58	3.92
NOR	50.35	4.36	NAI	60.92	-3.88
NDI	14.58	5.22	MSH	20.17	3.60
NAI	60.92	4.55	MAT	41.30	3.97
MSH	20.17	4.05	NIL	12.23	3.79
MAT	41.30	-4.34	KEV	40.17	-4.18
KEV	40.17	4.24	JER	40.31	-3.58
JER	40.31	4.43	IST	41.00	-3.59
IST	41.00	4.68	HLW	44.13	-3.64
HLW	44.13	-4.83	BUL	80.58	-4.68
HKC	31.59	-5.00	ALQ	103.00	-4.73
GDH	64.84	-4.73	CHG	26.18	3.82
BUL	80.58	4.46	KIP	94.44	-5.57
ALQ	103.00	4.58	KON	47.73	-4.48
CHG	26.18	4.65	OGD	95.19	-4.85
COL	65.86	4.88	TOL	64.00	-4.39
KBL	14.23	4.96	ALQ	103.00	-4.86
KIP	94.44	-6.04	CHG	26.18	3.72
KON	47.73	5.00	CTA	84.00	-3.89
OGD	95.19	-5.40	FBK	66.00	4.39
TOL	64.00	4.96	KIP	94.44	4.21
			KON	47.73	4.46
			OGD	95.20	4.54
AVERAGE		4.52			3.90

- minus sign by magnitude means it is an upper limit based on noise measurement since signal was not observed

TABLE III (Continued)

MAGNITUDE DATA FOR TIEN SHAN EARTHQUAKES

EVENT = 58

STATION	DELTA	m_b	STATION	DELTA	M_s
SHK	35.03	-4.67	SHK	35.03	-3.48
ASP	78.80	-4.10	BUL	83.83	-4.88
BUL	83.38	-5.05	CTA	82.38	-4.97
CTA	82.28	-4.74	GDH	64.22	-3.91
GDH	64.22	-5.30	HKC	29.87	-4.66
HKC	29.87	-5.95	HLW	47.05	-3.69
HLW	47.05	-5.27	IST	43.39	-3.63
IST	43.39	-4.62	JER	43.23	-3.63
JER	43.23	4.87	KEV	40.29	4.35
KEV	40.29	-4.10	MAT	38.14	-3.71
NIL	15.48	4.33	SNG	37.63	-4.13
MAT	38.14	-4.24	NAI	64.22	-4.22
SNG	37.63	-4.77	NDI	17.35	-3.45
MSH	23.32	4.90	NUR	41.10	-3.89
NAI	64.22	-4.82	POO	27.80	-3.91
NDI	17.35	4.20	QUE	21.74	3.53
NUR	41.10	4.50	SHI	31.85	-3.71
POO	27.80	-5.22	STU	52.98	4.63
QUE	21.74	4.43	UME	42.86	-3.66
SHI	31.85	-4.52	ALQ	101.00	-4.24
SHL	18.03	4.30	CHG	26.08	-3.44
STU	52.98	-4.52	COL	63.39	3.98
UME	42.86	4.62	CTA	82.38	-4.94
ALQ	101.00	-4.24	KBL	17.54	3.49
CHG	26.08	4.46	KIP	91.16	-5.07
CTA	82.38	-4.64	KON	48.64	-4.19
KBL	17.54	3.72	OGD	94.53	-4.19
KIP	91.16	-5.70	ALQ	100.00	3.96
KON	48.64	-4.84	CHG	26.10	3.40
OGD	94.53	-5.27	CTA	82.40	4.08
			KIP	91.20	3.58
			KON	48.64	4.02
			OGD	94.53	4.35
			TLO	65.70	3.92
AVERAGE		4.24			3.58

- minus sign by magnitude means it is an upper limit based on noise measurement since signal was not observed

TABLE III (Continued)

MAGNITUDE DATA FOR TIEN SHAN EARTHQUAKES

EVENT = 59

STATION	DELTA	m_b	STATION	DELTA	M_s
DAG	51.04	4.88	BUL	78.52	-4.36
BUL	78.52	4.65	CHG	26.37	4.10
CHG	26.37	4.56	COL	67.49	-4.65
COL	67.49	5.27	HKC	31.72	4.33
HKC	32.72	-5.65	IST	39.61	-3.57
IST	39.61	-5.00	JER	38.54	-3.55
JER	38.54	-4.24	SNG	37.44	4.13
KEV	40.30	-5.08	NAI	58.84	-3.85
KBL	12.15	5.59	NDI	12.90	4.34
MAT	43.30	4.53	POO	23.47	4.30
SNG	37.44	4.50	SHI	26.60	-3.28
MSH	18.24	-5.55	SHL	17.34	4.15
NAI	58.84	-4.62	STU	50.49	-4.74
NDI	12.90	5.44	SHK	40.00	4.52
NUR	39.77	4.80	UME	42.00	-4.46
POO	23.47	5.46	ALQ	104.00	-4.81
QUE	16.38	4.82	KIP	96.52	-6.01
SHI	26.60	-4.28	ALQ	104.00	4.71
SHL	17.34	4.93	CHG	26.37	3.91
STU	50.49	4.70	KIP	96.52	4.27
SHK	40.00	-5.35	KON	47.32	4.72
UME	42.00	-4.68	OGD	95.68	4.82
ALQ	104.00	-4.82	TLO	62.90	4.06
KIP	96.52	-5.95			
AVERAGE		4.70			4.05

- minus sign by magnitude means it is an upper limit based on noise measurement since signal was not observed

TABLE III (Continued)

MAGNITUDE DATA FOR TIEN SHAN EARTHQUAKES

EVENT = 60

STATION	DELTA	m_b	STATION	DELTA	M_s
UME	41.94	5.10	CTA	84.96	4.26
ASP	80.40	4.72	EIL	39.79	4.15
BUL	78.57	5.27	KIP	96.48	4.35
CHG	26.41	5.17	MAT	43.26	4.23
COL	67.42	5.63	TLO	62.88	4.15
HKC	32.75	-5.03	BUL	78.57	-4.66
IST	39.60	5.14	CHG	26.41	4.21
JER	38.54	4.45	COL	67.42	4.65
KEV	40.24	5.25	GDH	65.30	4.88
MAT	43.26	4.38	HKC	32.75	4.56
SNG	37.50	4.94	IST	39.60	3.87
MSH	18.26	-4.96	JER	38.54	4.20
NAI	58.88	-5.02	KEV	40.24	4.80
NDI	12.97	5.63	MAT	43.26	4.18
NOR	50.98	5.60	SNG	37.50	4.28
NUR	39.72	5.28	MSH	18.26	3.68
POO	23.53	5.34	NAI	58.88	4.23
QUE	16.42	4.76	NDI	12.97	4.22
SHI	26.62	4.70	NOR	50.98	4.35
STU	50.46	5.18	POO	23.53	3.97
SHK	39.97	4.66	QUE	16.42	4.07
			STU	50.46	4.72
			ALO	104.00	4.73
			CHG	26.41	4.23
AVERAGE		5.00			4.33

- minus sign by magnitude means it is an upper limit based on noise measurement since signal was not observed

TABLE III (Continued)

MAGNITUDE DATA FOR TIEN SHAN EARTHQUAKES

EVENT = 63

STATION	DELTA	m_b	STATION	DELTA	M_s
GDH	62.73	-5.23	EIL	39.69	3.63
NIL	12.02	4.20	KIP	95.15	4.08
BUL	80.05	4.83	KON	45.19	4.68
CHG	28.65	4.32	KON	45.19	4.43
CTA	86.54	4.62	MAT	42.97	4.09
HKC	34.13	5.18	ALQ	101.00	4.52
IST	38.62	4.92	TLO	61.38	4.02
KEV	37.81	4.83	OGD	93.07	4.20
MAT	42.97	4.17	BUL	80.05	-4.37
SNG	39.86	-5.04	CTA	86.54	-4.43
MSH	18.54	-4.98	HKC	34.13	4.44
NAI	60.16	-4.94	IST	38.62	-3.55
NUR	37.62	5.37	KEV	37.81	4.21
QUE	17.91	3.97	MAT	42.97	-3.93
SHI	27.21	4.70	SNG	39.86	-3.87
STU	48.80	5.08	NAI	60.16	-3.87
			QUE	17.91	3.94
			SHI	27.21	4.12
			STU	48.80	-4.32
			COL	65.08	-4.77
			CTA	86.54	4.06
AVERAGE		4.66			4.03

- minus sign by magnitude means it is an upper limit based on noise measurement since signal was not observed

TABLE III (Continued)

MAGNITUDE DATA FOR TIEN SHAN EARTHQUAKES

EVENT = 64

STATION	DELTA	m_b	STATION	DELTA	M_s
BUL	82.90	5.09	CHG	26.77	3.96
CHG	26.77	4.86	MAT	39.38	-4.16
MAT	39.38	4.28	MAT	39.38	4.11
DAG	49.08	4.61	ALQ	101.00	4.47
SNG	38.26	-4.77	CHG	26.77	3.99
COL	63.73	5.17	CTA	83.52	4.36
CTA	83.52	5.00	KIP	92.15	4.25
HKC	31.02	-4.97	TLO	64.52	4.24
IST	42.11	5.67	COL	63.73	4.51
KEV	39.52	4.52	CTA	83.52	-4.80
MSH	22.08	5.33	HKC	31.02	4.37
NAI	63.20	5.35	IST	42.11	-4.61
NUR	40.10	4.53	KEV	39.52	-5.04
SEO	30.82	-4.68	NAI	63.20	-3.90
SHI	30.66	4.49	NUR	40.10	-5.05
STU	51.83	-4.82	QUE	20.75	4.21
			SHI	30.66	4.21
			STU	51.86	-5.14
AVERAGE		4.80			4.14

- minus sign by magnitude means it is an upper limit based on noise measurement since signal was not observed

TABLE III (Continued)

MAGNITUDE DATA FOR TIEN SHAN EARTHQUAKES

EVENT = 65

STATION	DELTA	m_b	STATION	DELTA	M_s
BUL	79.91	4.38	KIP	95.16	4.85
COL	66.10	4.84	MAT	42.20	4.21
CTA	84.83	5.02	OGD	94.83	4.27
HKC	32.47	5.57	TLO	63.06	4.18
MSH	19.26	-5.23	COL	66.10	-4.94
NAI	60.19	-4.94	CTA	84.83	4.89
NUR	39.47	4.85	HKC	32.47	-4.02
SHI	27.74	-4.57	NAI	60.19	-4.17
STU	50.54	4.70	NUR	39.47	-4.86
			STU	50.54	-4.74
AVERAGE		4.89			4.48

- minus sign by magnitude means it is an upper limit based on noise measurement since signal was not observed

TABLE III (Continued)

MAGNITUDE DATA FOR TIEN SHAN EARTHQUAKES

EVENT = 66

STATION	DELTA	m_b	STATION	DELTA	M_s
			ALQ	102.00	4.47
			KON	49.28	-3.59
			OGD	95.43	4.16
			TLO	66.13	-3.65
			LAS	90.05	-4.13
			ALP	63.96	-2.45
			NOR	48.34	-2.96
AVERAGE	(NEIS)	5.00			3.28

- minus sign by magnitude means it is an upper limit based on noise measurement since signal was not observed

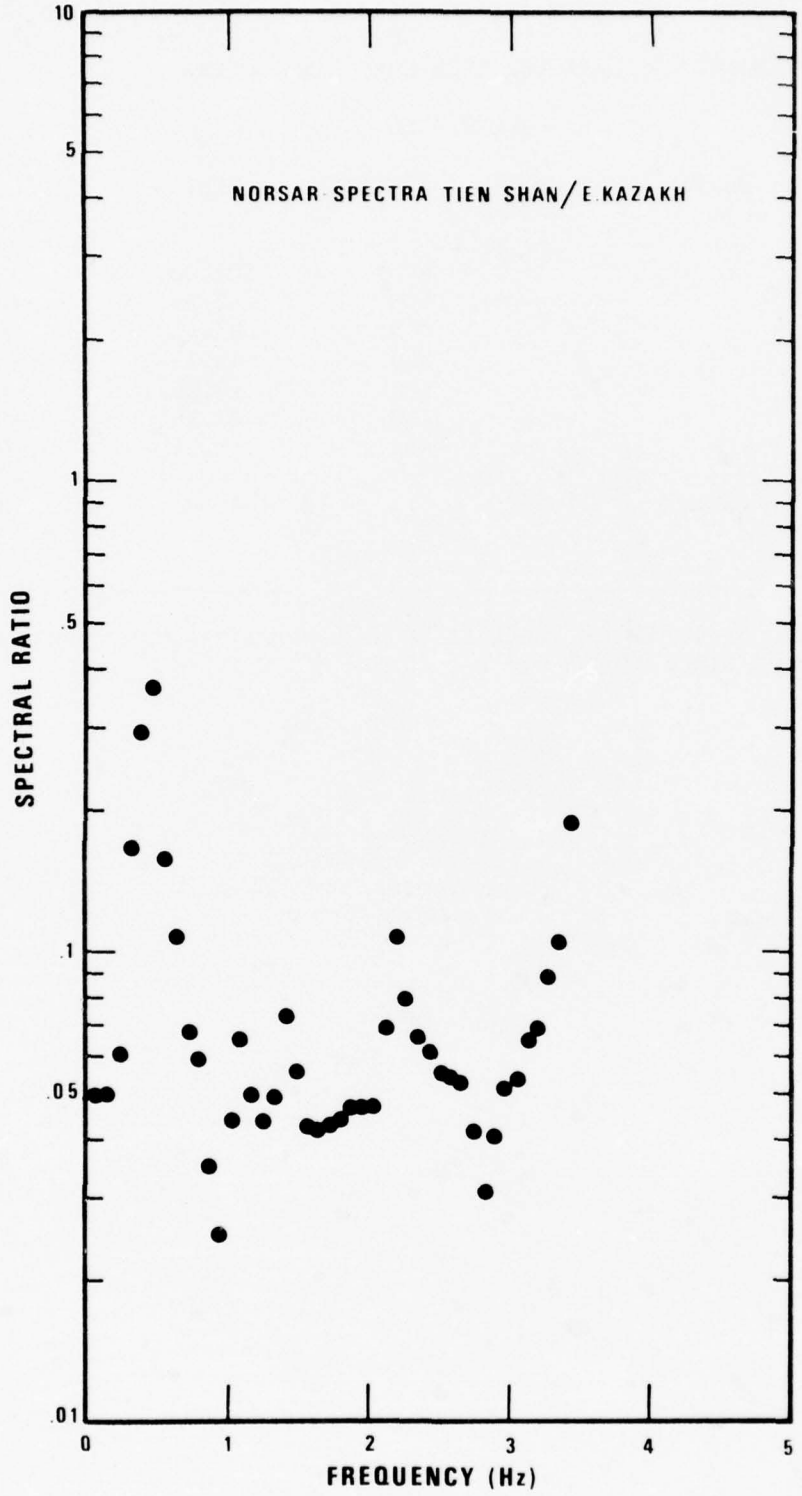

Figure 6. Ratio of average Tien Shan earthquake spectra to average Kazakh explosion spectra recorded at NORSAR.

average spectra of four large Kazakh explosions recorded at NORSAR. The average spectral ratio is less than 1 because the C3 subarray shows larger S/N ratios than the full array when recording East. Kazakh data. Also the East. Kazakh signals are about 0.5 m_b units larger than the Tien Shan signals, and in addition the path from Kazakh to NORSAR is a low attenuation path across the Eurasian shield. We assume that both the earthquakes and the explosions have the same source spectral shape over the band used to find $\underline{m}$; that is, a high-frequency asymptotic slope of ω^{-2}. The slope of the spectral ratio is almost zero from the corner frequencies at .5 to 1.0 Hz out to 3.5 Hz where the S/N ratio starts to drop. It follows that t* for the path from the Tien Shan to NORSAR is roughly the same as for the path from Kazakh to NORSAR. We emphasize that this is only a gross determination since the large relative amplitude difference at C3 between Kazakh and Tien Shan signals must be reflected in the spectra to some unknown degree. This value of t* corresponds to an average Q of 2600 or a relatively low attenuation path from the Tien Shan to NORSAR. This is consistent with our inference of high velocities there. In order to find t* for the Tien Shan to LASA path it was necessary to first find t* for the Kazakh to LASA path. von Seggern and Sobel (1976) have found t* for the Kazakh to LASA path to be 0.44. Figure 7 shows the ratio of the average spectrum of Tien Shan events recorded at LASA divided by the average spectrum of the Kazakh events recorded at LASA. Again the slope of the spectral ratio is approximately zero and t* for the path from the Tien Shan to LASA is taken to be 0.44. This value of t* corresponds to a Q of 1800 or a relatively low attenuation path again. The scatter of the data is too large, though, to establish with high confidence a real difference between these values of Q for the two paths from the Tien Shan to LASA and NORSAR. Yet, examination of signals in Figure 3 affirms that the NORSAR recordings have a higher frequency content, and therefore higher Q.

von Seggern and Sobel (1975) have presented a method of predicting 20-second Rayleigh-wave amplitudes by geometrical ray tracing. Their work shows that lateral changes in 20-second LR-phase velocity can cause multipathing and large teleseismic amplitude variations due to small-scale refraction effects. In Figures 8 and 9 we illustrate the pattern of rays which

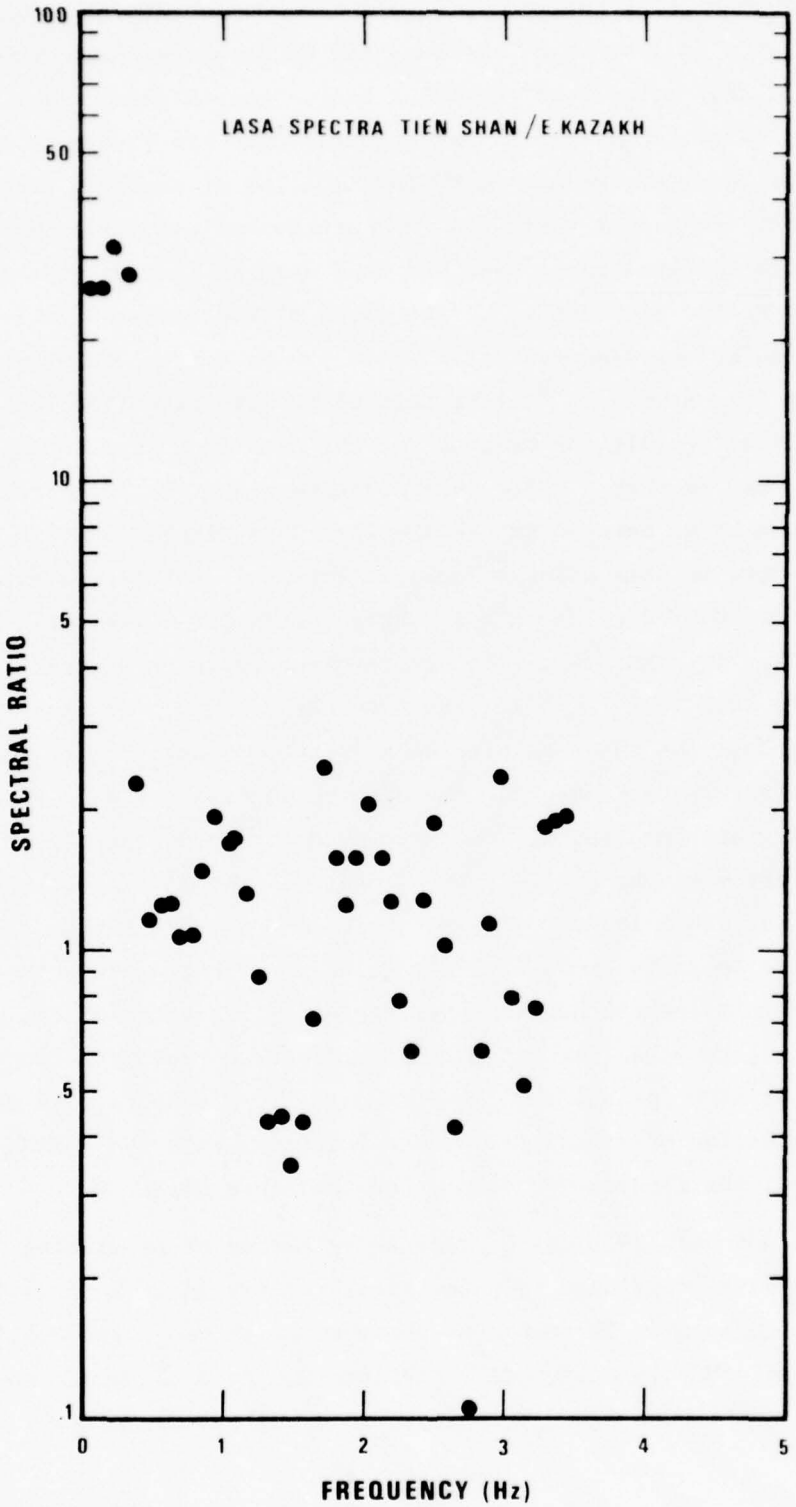

Figure 7. Ratio of average Tien Shan earthquake spectra to average Kazakh explosion spectra recorded at LASA.

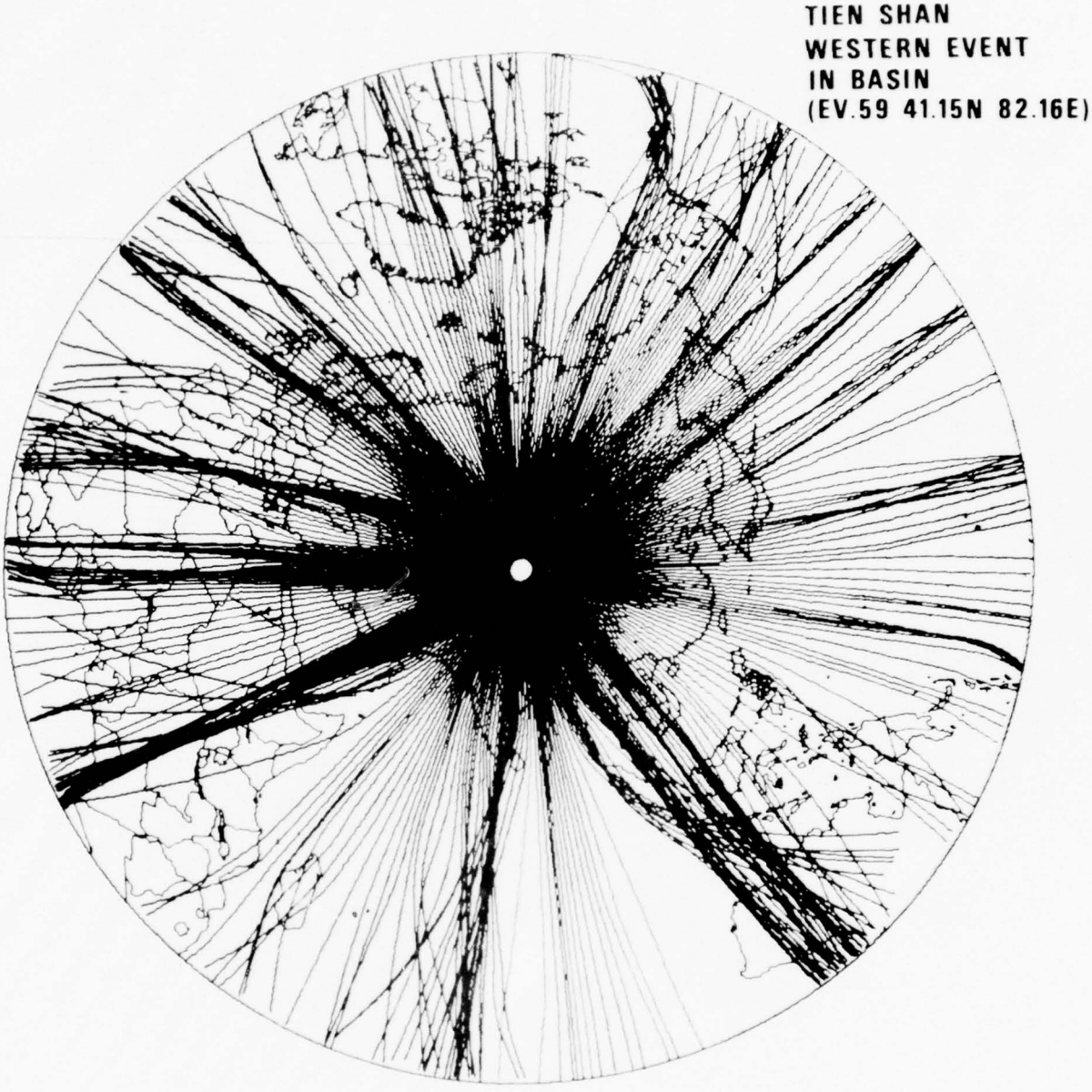

Figure 8. Predicted LR raypaths (T=20 sec) from event 59.

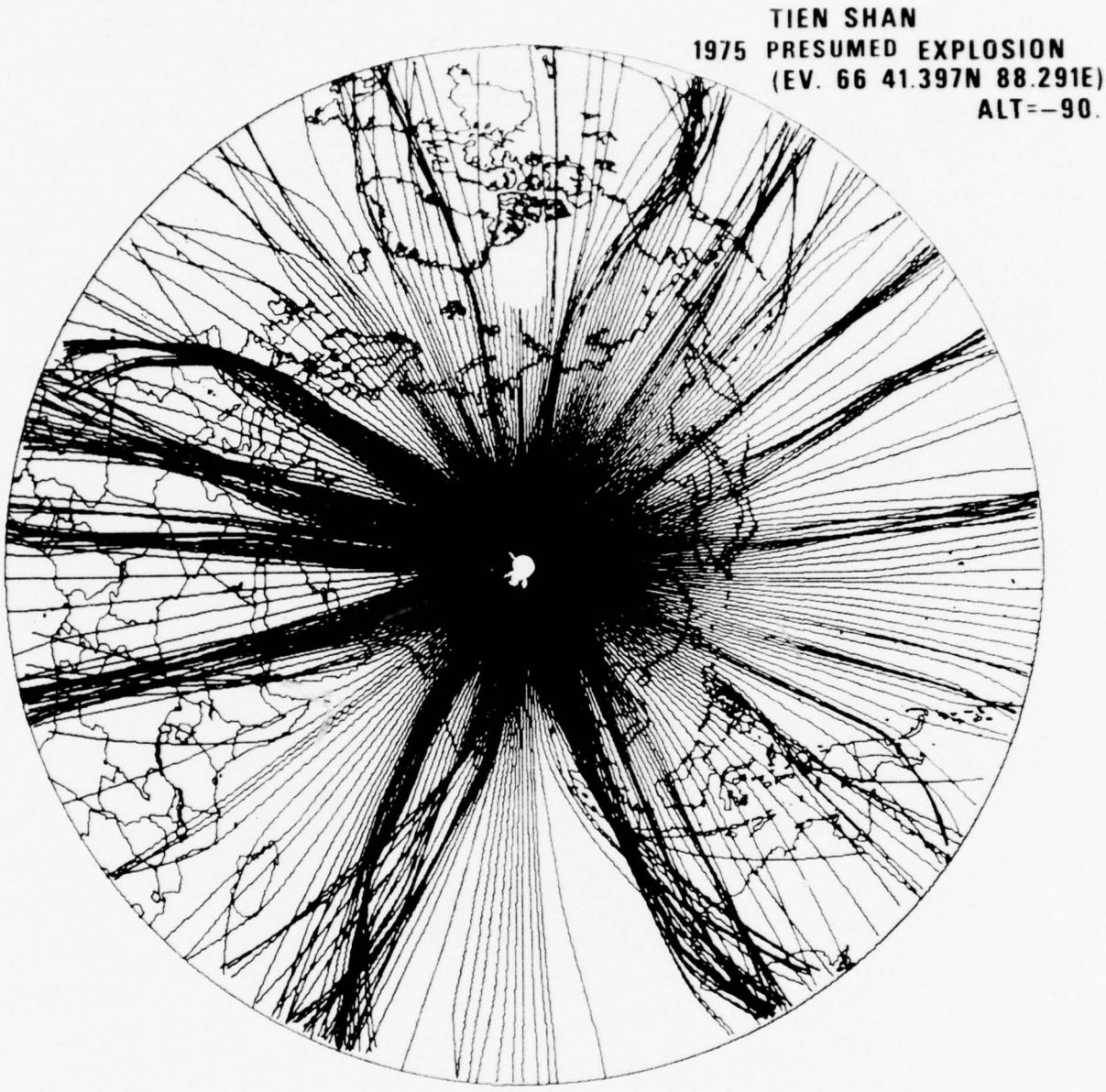

Figure 9. Predicted LR raypaths (T=20 sec) from event 66.

results for event 59, located in the west of our region of study, and event 66, located in the east of it, using the global velocity grid of von Seggern and Sobel. No attempt is made here to quantitatively relate these patterns to observed LR amplitudes since we cannot correct the predicted amplitudes for source mechanism. Note that both figures show large amplitudes in Central and Northern Africa, western British Columbia and western Australia. Another important point is that certain stations will see large amplitude variations between epicenters located in the eastern versus the western part of the Tien Shan. For example, NORSAR would record higher amplitudes for events in the western part of the Tien Shan than for identical-size events in the eastern part. Stations which record a stable amplitude are desirable for calibrating a source region for amplitude. For events from the Tien Shan region, such stations could be located in southeastern China, the eastern USSR and the central Pacific Basin. The complicated LR ray-tracing figures partially explain why we were unable to determine LR radiation patterns from our amplitude observations.

DISCRIMINATION ASPECTS

M_s-m_b

In this and following sections we apply several common discriminants between earthquakes and explosions to the Tien Shan events. We had chosen those events which, during preliminary screening, were of low M_s for their m_b. Then we independently determined average M_s and m_b values for the Tien Shan events in Table II using WWSSN stations, HGLP stations, and the LASA and NORSAR arrays. The data used in the average estimates is listed in Table III. Negative values in the table indicate noise measurements were used as upper bounds for the signal amplitudes. Magnitudes were computed according to the formulas

$$m_b = \log(A/T) + B(\Delta)$$
$$M_s = \log(A/T) + 1.66 \log\Delta + 0.3$$

where

A = one-half the peak-to-peak maximum record amplitude reduced to mμ ground displacement,

T = period in seconds (restricted to 17-23 sec for M_s calculation),

Δ = epicentral distance in degrees,

B(Δ) = Gutenberg-Richter correction term for P waves.

We have used a method of magnitude averaging proposed by Ringdal (1976), which includes noise measurements as upper bounds to produce the M_s-m_b plot in Figure 10. Note that for some of the events in Table III half the readings are noise levels. The magnitude averages of these events should be lower than what would result if only measured signal amplitudes were used (Ringdal, 1976). The line $M_s = m_b - 1.0$ in Figure 10 lies below all events in that plot except event 53, which lies close to the line, and event 66 which lies below the line. All the Tien Shan events except event 66 lie above the line $M_s = 1.28\ m_b - 2.91$, which is one suggested decision line for Western United States earthquakes and explosions (Basham and Horner, 1973). Also plotted in Figure 10 are 15 Semipalatinsk explosions, which are located about 10 degrees northwest of the Tien Shan events. The M_s and m_b values are from von Seggern (1976). All the explosions clearly lie below the line $M_s = m_b - 1.0$ as would be expected for explosion data, and event 66 clearly lies within the explosion population.

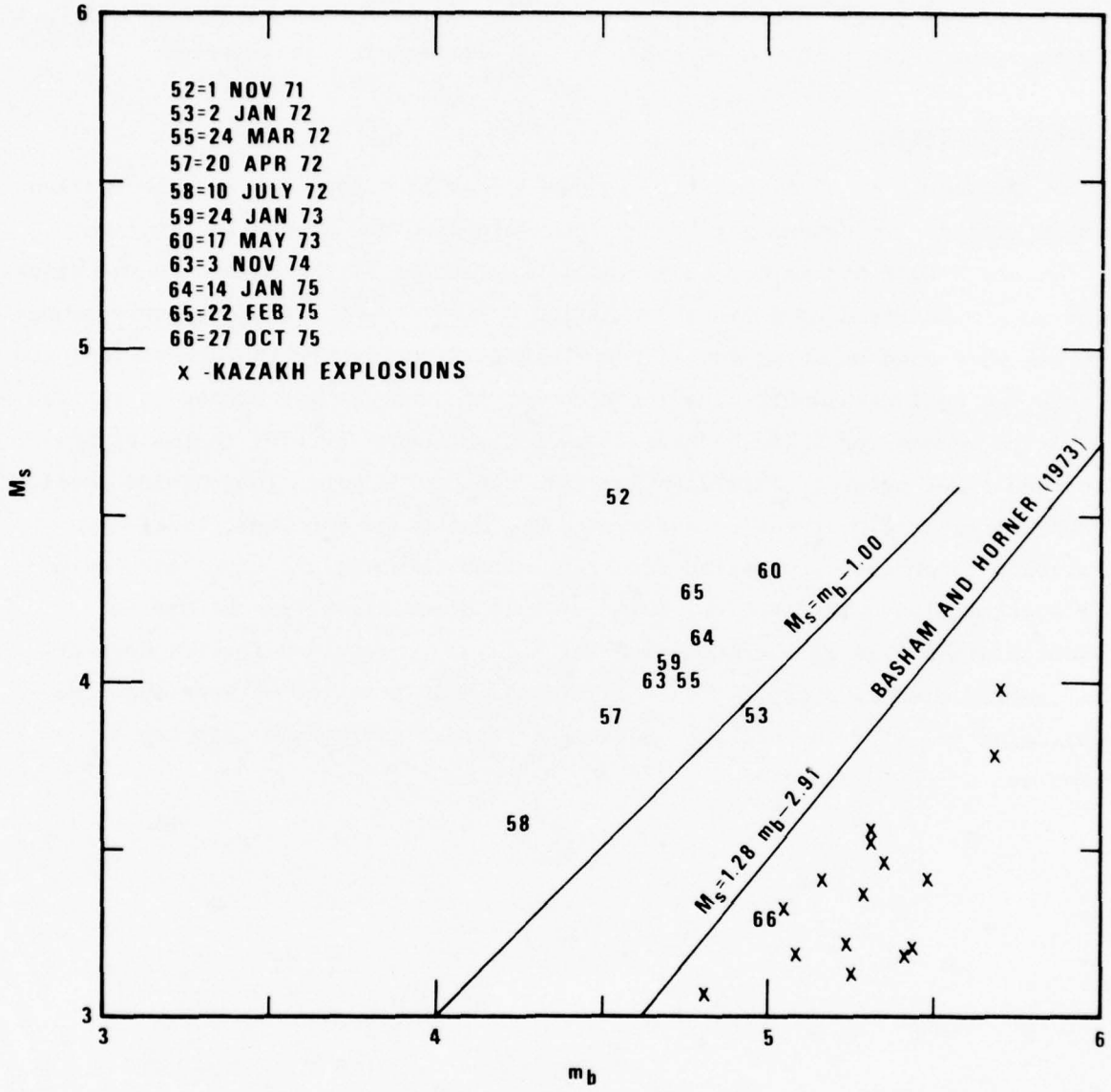

Figure 10. M_s vs. m_b for Tien Shan earthquakes.

Event 60 would be expected to lie below most of the earthquake population if it truly had an ISC reported depth of 96 km; in fact, its position in the M_s-m_b plot is in accord with our previous argument for shallower depth.

Corner Frequency

Figure 11 is a plot of $|\hat{u}_o|$ versus corner frequency for the eleven Tien Shan events. Unfortunately no P phases were recorded at the long-period LASA and NORSAR arrays due to the small magnitudes of the events so the values of $|\hat{u}_o|$ were found from the short-period spectral data. Where noise measurements were used as upper bounds for the signal amplitude, the arrows indicate that the real data would have lower corner frequencies and higher $|\hat{u}_o|$. The average values for 4 Kazakh explosions and our event 66 plot to the right of the other points. This data suggests that for a given long-period level, explosions have a higher corner frequency; Hanks and Thatcher (1972) have already shown such separation for Aleutian earthquakes and explosions using P spectra also. The physical basis of this discriminant is the smaller source dimensions of the explosion for a given long-period level. However, if source dimension $a \propto \alpha/f_c$, then Figure 11 shows a factor of less than two differences, if α is constant, between a typical earthquake near Lop Nor and an explosion there.

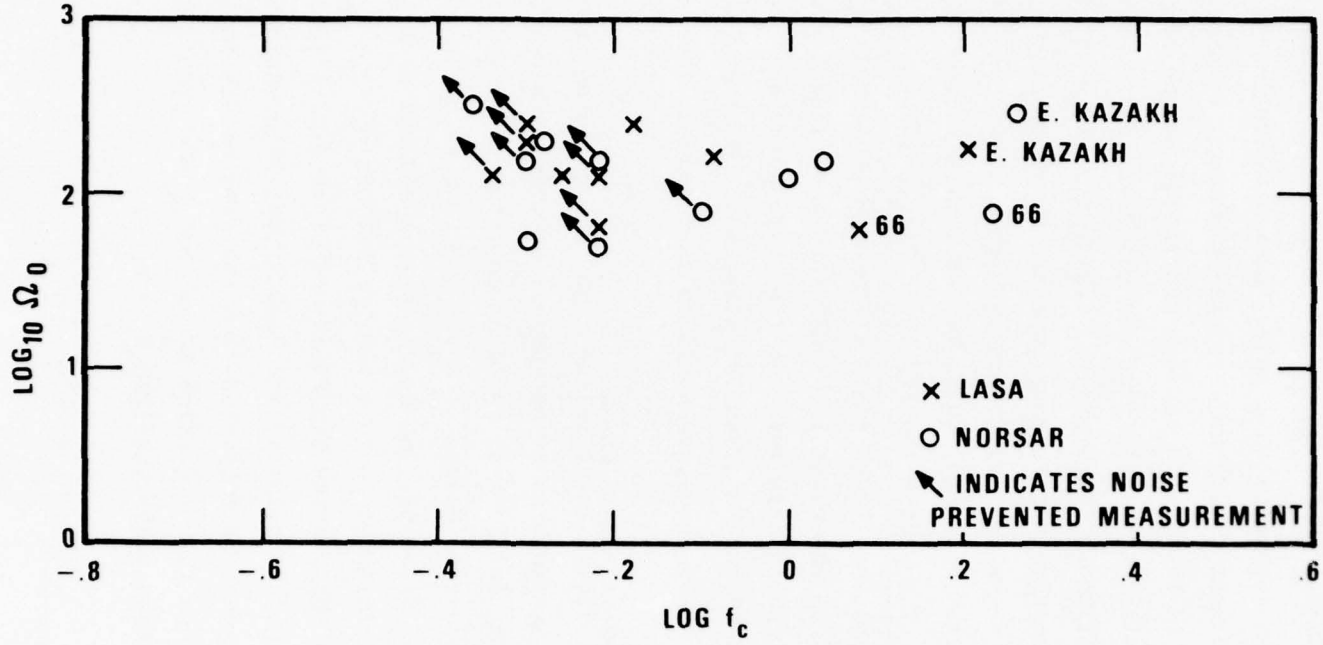

Figure 11. Long-period spectral level vs. corner frequency for Tien Shan events from LASA and NORSAR P recordings.

Long-Period Body-wave Excitation

For the eleven events of this study, we have compiled in histogram form the ground displacement ratios of vertical-component, long-period S and P waves to LR waves in Figures 12 to 14. The ratios may be compared to the distributions obtained from LRSM stations using worldwide events by von Seggern (1972). Although there are too few observations in the Tien Shan data set to confidently compare their medians to those of von Seggern, the Tien Shan log (S/LR) values are generally higher than those for NTS explosions recorded at LRSM stations, which lie at approximately -1.2 in von Seggern's histogram. The medium log (P/LR) in Figure 14 lies at roughly -.4, which is the same as that found for the Kamchatka earthquakes by von Seggern and Sobel (1976) and which is higher than indicated for worldwide earthquakes by von Seggern. There were too few LQ observations to determine ratios of long-period LQ and LR ground displacement. Most of the LQ observations were close to the noise level, as would be expected for these small magnitude events.

A more useful discriminant is the magnitude computed from long-period body waves since this entails no dependence on epicentral distance. Average values of m_b for S waves could be computed for only five of the eleven Tien Shan events. Values of $\bar{m}_b(S) - \bar{M}_s$ are shown in the Table IV for these five events. Event 66, the only possible explosion of the eleven events we studied, is not included in this table. All the $\bar{m}_b(S) - \bar{M}_s$ values in Table IV are larger than -0.2, which Blandford and Clark (1974) found to be the largest value for Amchitka Island and Nevada Test Site explosions. Only three $\bar{m}_b(P) - \bar{M}_s$ values could be determined for the five events in Table IV. All three values are less than 1.0 which means that these events lie within the earthquakes population above the line $M_s = m_b - 1$.

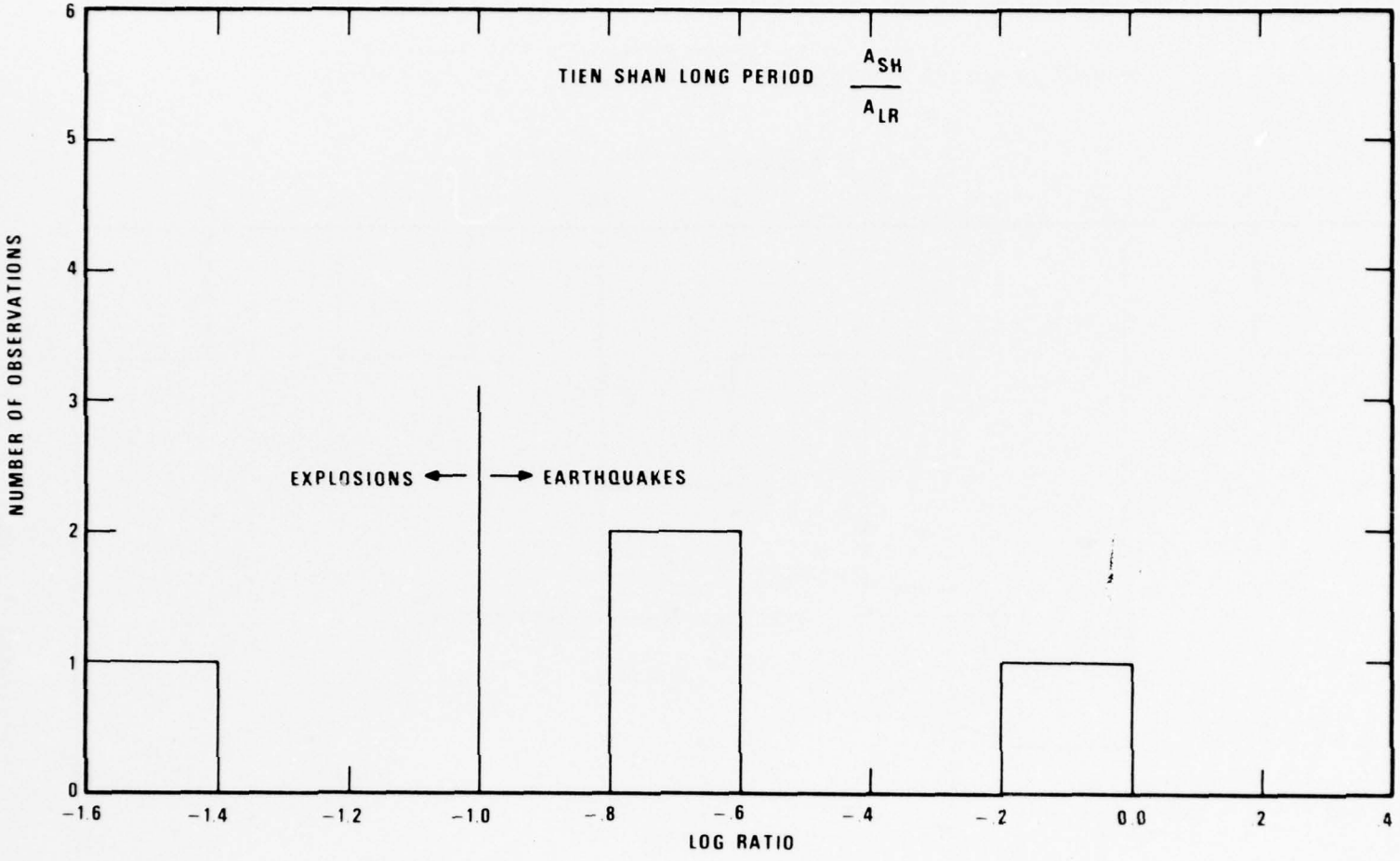

Figure 12. Distribution of log (SH/LR) for ratio of ground displacement from Tien Shan events.

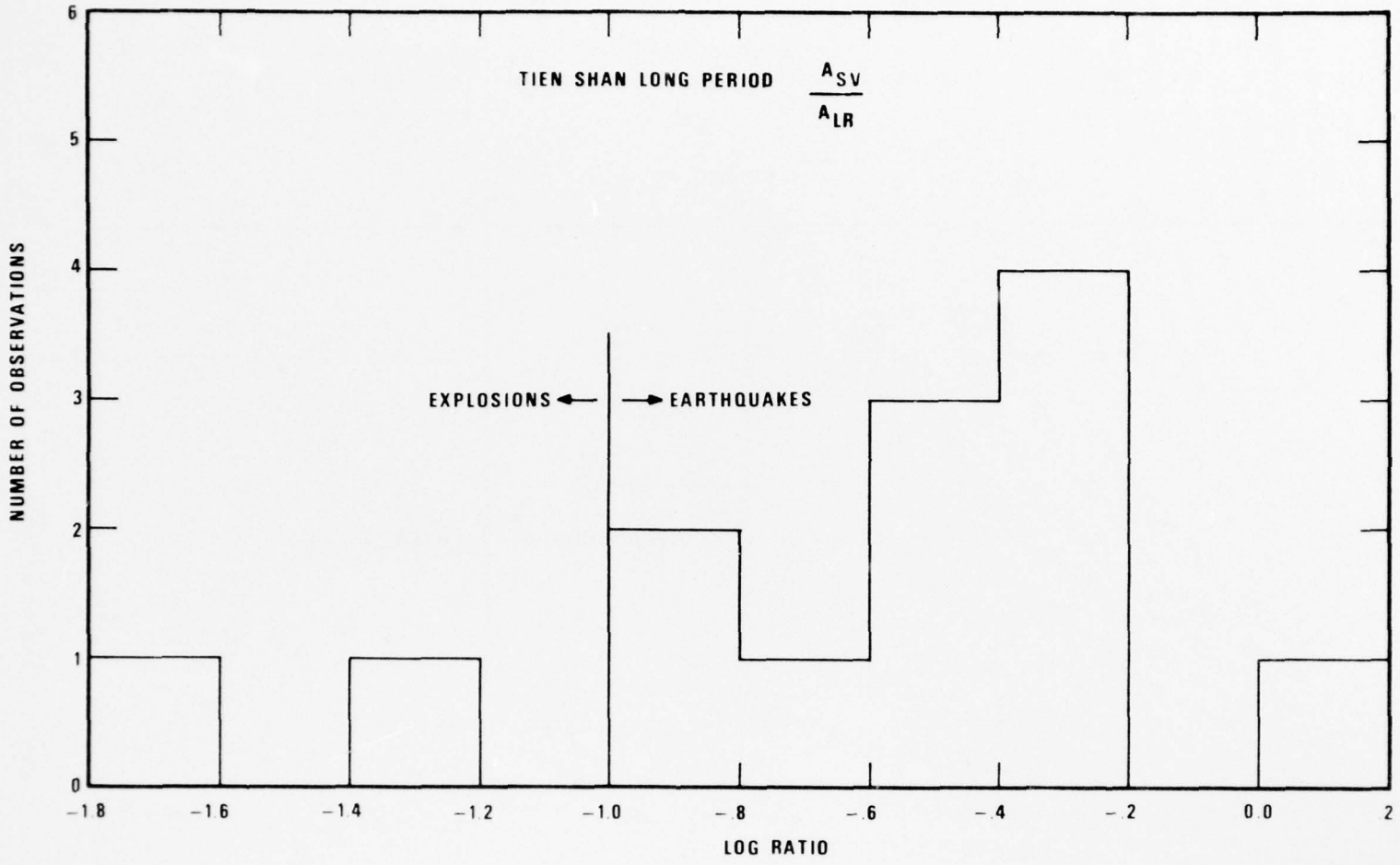

Figure 13. Distribution of log (SV/LR) for ratios of ground displacement from Tien Shan events.

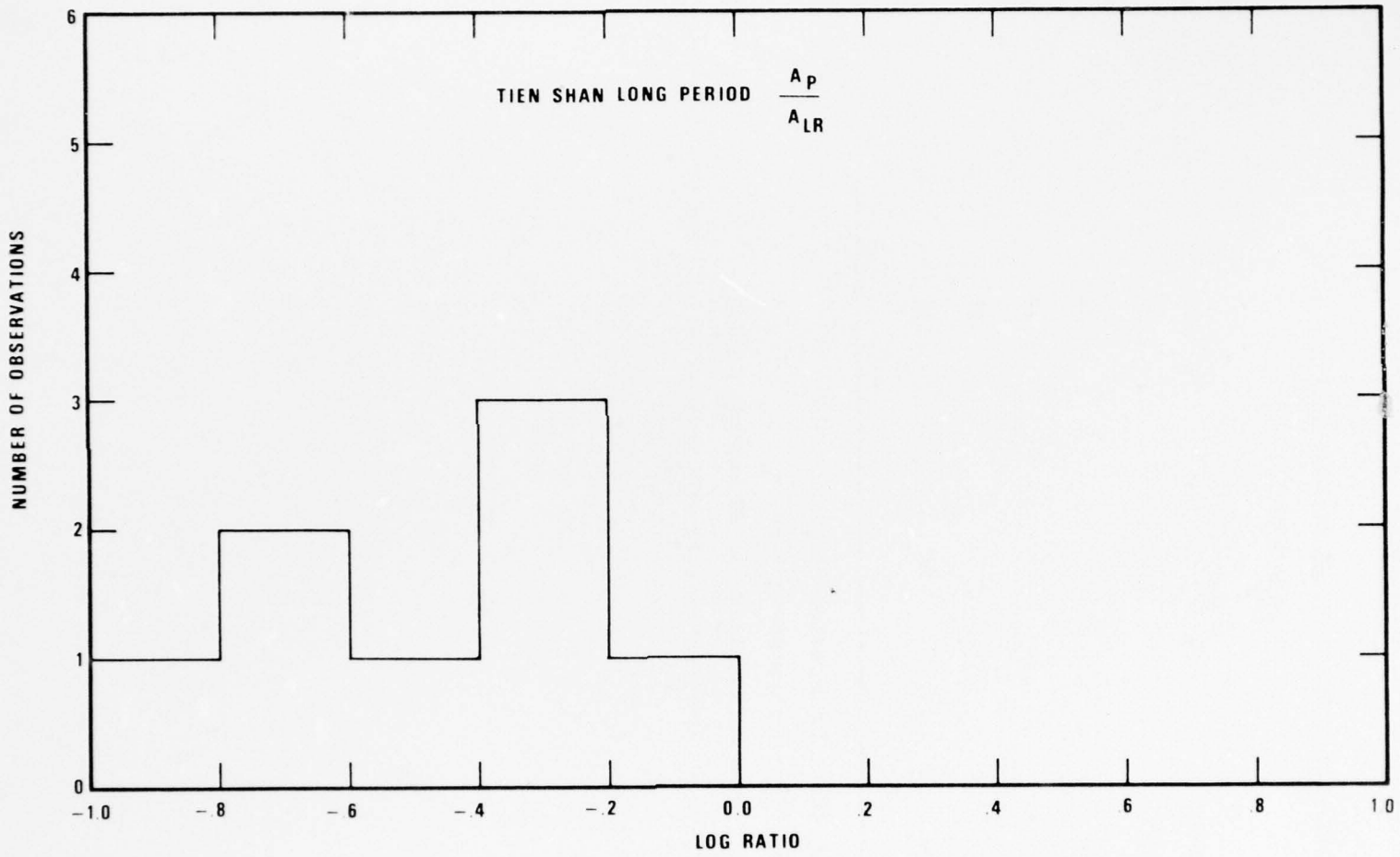

Figure 14. Distribution of log (P/LR) for ratios of ground displacement from Tien Shan events.

TABLE IV

LONG-PERIOD BODY-WAVE MAGNITUDES RELATIVE TO M_S
FOR TIEN SHAN EARTHQUAKES

Event	$\overline{m_b\ (P)} - \overline{M_s}$	$\overline{m_b\ (S)} - \overline{M_s}$
52	-.02	.45
53	—	-.01
55	.56	.73
58	—	-.16
60	.97	.31

---

m_b (P) - long-period P-wave m_b
m_b (S) - long-period S-wave m_b
M_s - LR magnitude at 20 seconds period
— - denote averaging over available readings for each event

Depth of Focus

Of the eleven events studied here, all but event 66 had apparent pP phases recorded at either LASA or NORSAR or both arrays. Many low $M_s - m_b$ events in this region could be identified as earthquakes on the basis of pP, assuming that other stations could corroborate LASA and NORSAR pP detections. An aspect of focal depth which can serve as a discriminant is the generation of higher mode LR. Higher modes were observed for several low M_s earthquakes in Tibet by Tatham et al. (1976) on SHL seismograms. We were unable to positively detect any higher modes for our events on seismograms selected for this study; however, our closest station, (SHL) also was much more distant than those used for the Tibet epicenters by Tatham et al.

Complexities

We have computed the "complexity" parameter as seen at LASA and NORSAR for the Tien Shan earthquakes in the manner given by Lambert et al. (1969). Table V lists the computed values. LASA beams show clear pP signals for 3 events and NORSAR beams show clear pP signals for 6 events. We believe that the lack of a clear pP signal in the other cases was due to noisy data or to a pP signal that could not be visually separated from the P coda. Larger complexity numbers, and therefore higher coda energy, were associated with positive pP detections. The complexity numbers for a set of 4 Kazakh explosions were low (1.83 - 2.39), as would be expected for an explosion. Event 66, already having shown explosion characteristics, falls within the complexity range for earthquakes, thus indicating the unreliability of complexity measurements.

Spectral Ratios

Spectral ratios have been calculated at LASA and NORSAR according to a form suggested by Lacoss (1969)

$$R = \int_{1.55}^{1.95} A(f)df \Big/ \int_{.45}^{.85} A(f)df$$

where sums of the equivalent terms of the discrete Fourier transform have replaced the integrals. These ratios are plotted against m_b for the eleven Tien Shan events and also for 4 Kazakh explosions in Figure 15.

TABLE V

COMPLEXITIES FOR TIEN SHAN P WAVES

EVENT	LASA	NORSAR
52	—	4.11
53	2.99	4.48
55	4.88	9.50
57	3.39	4.10
58	4.79	6.82
59	3.19	5.80
60	6.69	5.86
63	3.06	—
64	—	9.59
65	9.74	3.30
66	6.04	5.40

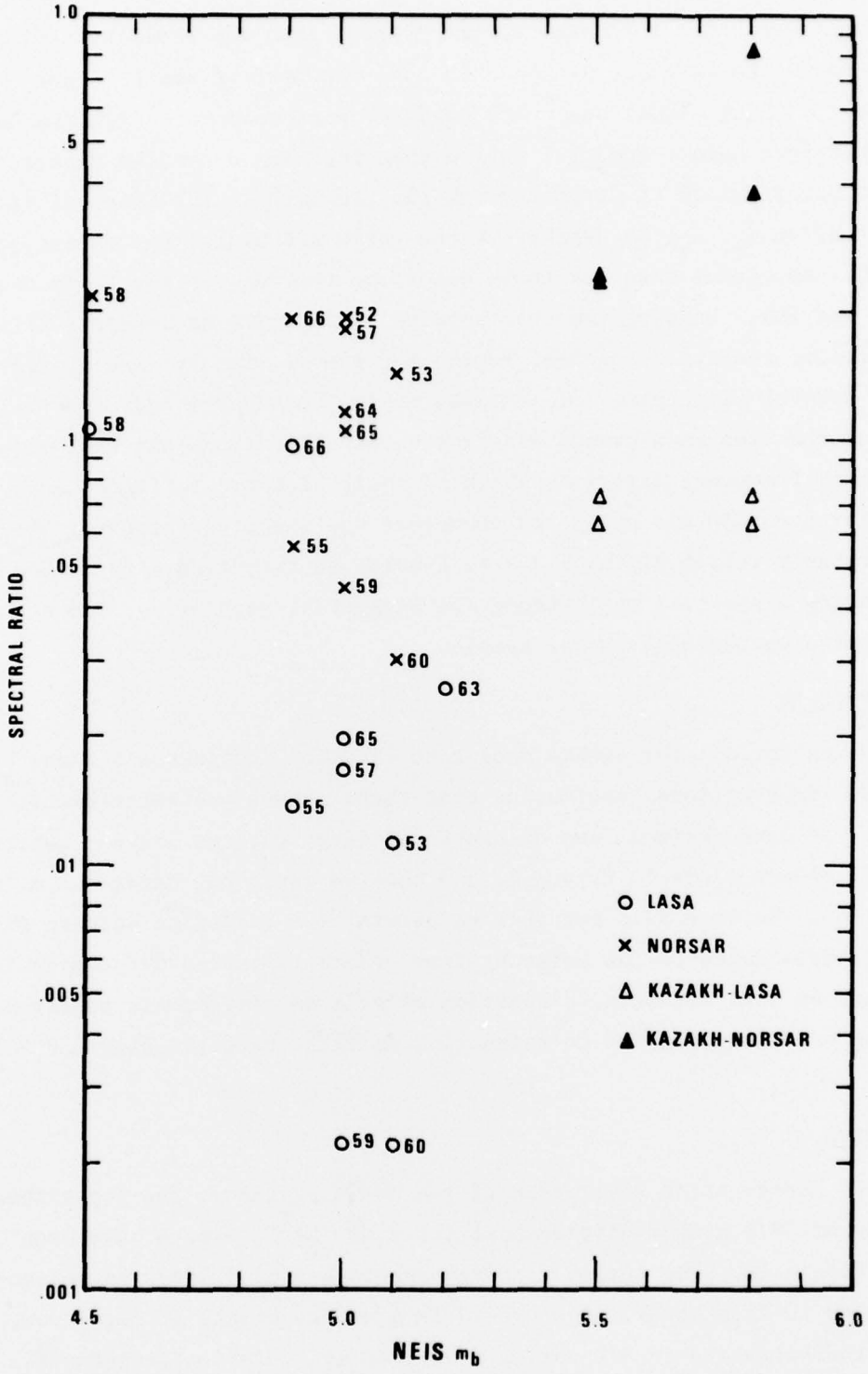

Figure 15. Short-period P spectral ratio vs. m_b for Tien Shan events recorded at NORSAR and LASA.

The amplitudes of the P spectra were greater than the amplitudes of the noise spectra in the frequency range 0 to 5 Hz for most of the LASA and NORSAR beams. NORSAR signal beams (C3 subarray possessed more high frequencies and therefore higher spectral ratios than the LASA beams (A0 subarray, in accord with our previous t* estimates for the two paths. The spectral ratio did not depend on m_b, M_s, or depth; but the ratio was higher for events in the Tien Shan mountains than for those events on the edge of the Tarim Basin (events 59 and 60). Passing the data through a 0.4 - 3.0 Hz bandpass filter produced similar results. Spectral ratios for the pP signals were similar to the ratios for the main phase. The Kazakh explosions show larger spectral ratios than most of the Tien Shan events as might be expected since the explosions contain more high frequency energy as shown by their higher cutoff frequency. The LASA beam for event 58 was noisy and therefore the spectral ratio for that beam was probably relatively high due to a noise contribution. Event 66, although having a spectral ratio among the highest at each array, did not separate from the earthquakes in our sample.

Radiation Pattern

Body waves for all the events except 66 show both compressional and dilatational first motions, indicating that these events are earthquakes. Unfortunately the compressional and dilatational first motions did not separate on the focal sphere plots in Figure 2, and thus we could not determine a fault plane solution. We were also not able to determine a radiation pattern from the LR amplitudes owing to the large scatter, which is caused by propagation effects, such as Q differences, dispersion effects on time-domain amplitudes, and focusing or defocusing due to refraction as illustrated in Figure 8 and 9.

S/P Excitation

From the short-period recordings of the WWSSN stations, the logarithms of 15 ratios of SV/P ground displacement for 8 of the 11 events have been plotted in Figure 16. The remaining three events had no S waves on seismograms analyzed in this study. The spread is over two orders of magnitude, reflecting the variation in S/P ratios predicted by radiation patterns for

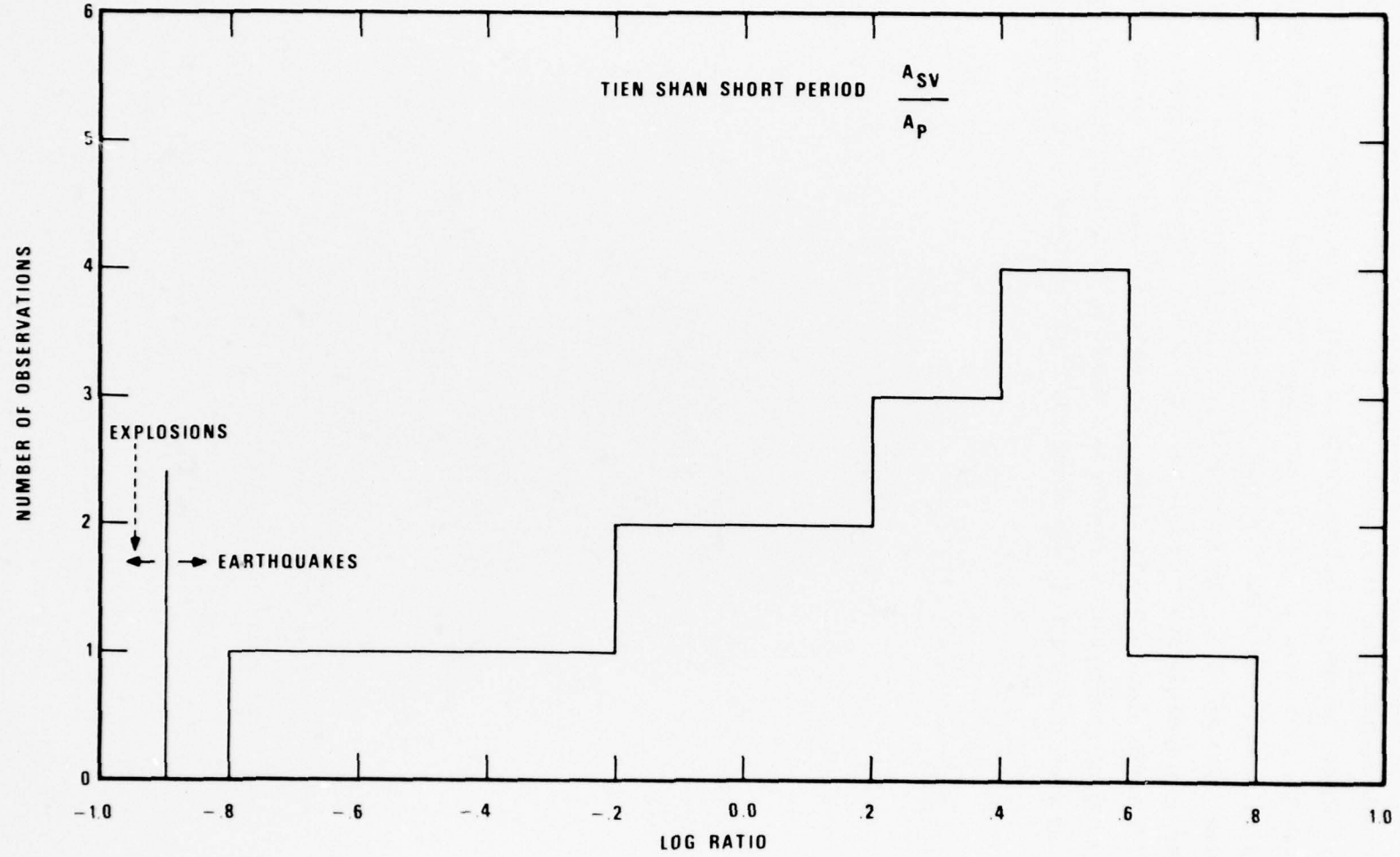

Figure 16. Distribution of ratio SV/P for ground displacement from short-period recordings of Tien Shan events.

double-couple models of an earthquake, plus the differential Q effects on P and S. Also, the spread is comparable to that shown by von Seggern (1972) for a much larger sample of global earthquakes recorded by the LRSM network. Von Seggern showed that a small sample of Nevada explosions plot with a median log (S/P) of -1.0. The median of our Tien Shan data lies at least one order of magnitude above the Nevada explosions. All those events with a log (SV/P) ratio above 0.0 certainly lie outside the range for explosions. Event 66 had no observable short-period S waves on recordings analyzed in this study even though its m_b was among the highest of the group selected.

SUMMARY

Eleven earthquakes with low reported M_s for their m_b from the area near Lop Nor in the eastern Tien Shan were examined in a seismic discrimination context. All the events lie close to major faults observed in satellite photographs. It was impossible on the basis of first motions to determine fault plane solutions owing to the insufficiently large magnitudes of the events. We were also unable to determine a radiation pattern from the LR amplitudes, probably due to varying propagation effects. The following characteristics of the Tien Shan events indicate that all the events are earthquakes, except event 66 on October 27, 1975, which is probably an explosion:

--When compared to 4 Kazakh explosions the Tien Shan events showed lower corner frequencies for the same seismic moment or long-period amplitude, except event 66 which was close to the Kazakh explosion population.

--All the Tien Shan earthquakes except event 66 fall on or above the line $M_s = m_b - 1.0$. Kazakh explosions clearly lie below the line $M_s = m_b - 1.0$ by 0.5 to 1.0 M_s units.

--The Tien Shan log (SV/LR) and log (P/LR) ratios of long-period ground displacement are generally larger than those for NTS explosions.

--The Tien Shan log (SV/P) ratios of short-period ground displacement are significantly larger than those for NTS explosions.

--All the earthquakes except event 66 had apparent pP phases recorded at LASA and/or NORSAR.

--Complexity numbers show larger coda energy for the Tien Shan events, including event 66, than for 4 Kazakh explosions.

--The Tien Shan events generally show smaller spectral ratios, or less high frequency energy, than Kazakh explosions.

--All the Tien Shan events except event 66 show some dilatational first motions, indicating that these events are earthquakes; however, the direction of the first motion is probably not reliable in all cases.

Although we have found that an explosion in the Lop Nor test area is easily classified as such within a small sample of earthquakes nearby, the explosion was a m_b = 5.0 event, and we cannot claim this reliability extends to lower magnitudes.

The installation of high-quality SRO stations in Asia will permit examination of lower magnitude events, and more importantly, with multistation, short-period digital data. Also, only one of the eleven earthquakes studied was very shallow in the crust, and the study of more such events would be desirable since discrimination should be most difficult for explosions and very shallow earthquakes.

REFERENCES

Alekseev, A., Belonosova, A., Burmakov, I., Krasnopevtseva, G. Matseeva, N. Nersessov, G., Pavlenkova, N., Ronanov, V. and V. Ryaboy, 1973. Seismic studies of low-velocity layers and horizontal inhomogeneities within the crust and upper mantle on the territory of the U.S.S.R., Tectonophysics, 20, 47.

Belyaevsky, N., Borisov, A., Fedynsky, V., Fotidati, E., Subbotin, S., and I, Volvosky, 1973. Structure of the Earth's crust on the territory of the U.S.S.R., Tectonophysics, 20, 35.

Basham, P. and R. Horner, 1973. Seismic magnitudes of underground nuclear explosions, Bull. Seism. Soc. Amer., 63, 105.

Ben-Menahem, A., Smith, S. and T. Teng, 1965. A procedure for source studies from spectrums of long-period seismic body waves, Bull. Seism. Soc. Amer., 55, 203.

Blandford, R. and D. Clark, 1974. Detection of long-period S from earthquakes and explosions at LASA and LRSM stations with application to positive and negative discrimination of earthquakes and underground explosions, SDAC Report No. TR-74-15, Teledyne Geotech, Alexandria, Virginia.

Hanks, T. and W. Thatcher, 1972. A graphical representation of seismic source parameters, J. Geophys. Res., 77, 4393.

Lacoss, R., 1969. A large-population LASA discrimination experiment, Technical Note 1969-24, Lincoln Laboratory, Lexington, Massachusetts.

Lambert, D., von Seggern, D., Alexander, S. and G. Galot, 1969. The LONGSHOT Experiment, Volume II. Comprehensive Analysis, SDL Report No. 234, Teledyne Geotech, Alexandria, Virginia.

Molnar, P. and P. Tapponnier, 1975. Cenozoic Tectonics of Asia: effects of a continental collisons, Science, 189, 419.

Noponen, I., 1975. Compressional wave power spectrum from seismic sources: June 30, 1972 - December 31, 1975, Advanced Research Project Agency, ARPA Order No. AO 2131-1, 66 pp.

Ringdahl, F., 1976. Maximum-likelihood estimate of event magnitude, Bull. Seism. Soc. Am., 66, 789.

Shirokova, E., 1967. General features in the orientation of principal stresses in earthquake foci in the Mediterranean-Asian seismic belt, Izvestia, Physics of the Solid Earth, 1, 12.

Tatham, R., Forsyth, D. and L. Sykes, 1976, The occurrence of anomalous seismic events in Eastern Tibet, Geophys. J. R. Astr. Soc., 45, 451.

Volarovich, M., Banyk, Y., Valyers, V. and I. Galkin, 1975. Seismic models of the crust from DSS data and laboratory measurements of the velocity of elastic waves, Izvestia, Physics of the Solid Earth, 11, 319.

von Seggern, D., 1976. Final report on the analysis of recordings from the Very Long Period Experimental Stations, SDAC Report No. TR-76-1, Teledyne Geotech, Alexandria, Virginia.

von Seggern, D., 1972. Seismic shear waves as a discriminant between earthquakes and underground nuclear explosions, SDL Report No. 295, Teledyne Geotech, Alexandria, Virginia.

von Seggern, D. and P. Sobel, 1975. Experiments in refining M_s estimates for seismic events, SDAC Report No. TR-75-17, Teledyne Geotech, Alexandria, Virginia.

von Seggern, D. and P. Sobel, 1976. Study of selected Kamchatka earthquakes in a seismic discrimination context, SDAC Report, Teledyne Geotech, Alexandria, Virginia.

York, J., Cardwell, R. and J. Ni, 1976. Seismicity and Quaternary faulting in China, Transactions, American Geophysical Union, 57, 332.

Zaychikov, V., ed., 1965. The Physical Geography of China, U.S. Department of Commerce, Joint Publications Research Service, JPRS: 32, 119, 650 pp.